Acta Pharmaceutica Sinica B 2022;12(6):2640–2657

Chinese Pharmaceutical Association
Institute of Materia Medica, Chinese Academy of Medical Sciences

Acta Pharmaceutica Sinica B

www.elsevier.com/locate/apsb
www.sciencedirect.com

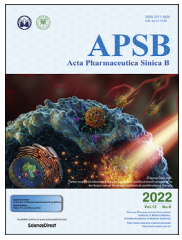

REVIEW

Chemotherapeutic nanomaterials in tumor boundary delineation: Prospects for effective tumor treatment

Ozioma Udochukwu Akakuru[a,†], Zhoujing Zhang[b,†], M. Zubair Iqbal[a,c], Chengjie Zhu[a], Yewei Zhang[b], Aiguo Wu[a,*]

[a]*Cixi Institute of Biomedical Engineering, International Cooperation Base of Biomedical Materials Technology and Application, Chinese Academy of Sciences (CAS) Key Laboratory of Magnetic Materials and Devices, Zhejiang Engineering Research Center for Biomedical Materials, Ningbo Institute of Materials Technology and Engineering, CAS, Ningbo 315201, China*
[b]*School of Medicine, Southeast University, Nanjing 210009, China*
[c]*School of Materials Science and Engineering, Zhejiang Sci-Tech University, Hangzhou 310018, China*

Received 29 October 2021; received in revised form 27 January 2022; accepted 6 February 2022

KEY WORDS

Bioimaging;
Boundary delineation;
Tumor;
Tumor imaging;
Tumor therapy;
Surgery

Abstract Accurately delineating tumor boundaries is key to predicting survival rates of cancer patients and assessing response of tumor microenvironment to various therapeutic techniques such as chemotherapy and radiotherapy. This review discusses various strategies that have been deployed to accurately delineate tumor boundaries with particular emphasis on the potential of chemotherapeutic nanomaterials in tumor boundary delineation. It also compiles the types of tumors that have been successfully delineated by currently available strategies. Finally, the challenges that still abound in accurate tumor boundary delineation are presented alongside possible perspective strategies to either ameliorate or solve the problems. It is expected that the information communicated herein will form the first compendious baseline information on tumor boundary delineation with chemotherapeutic nanomaterials and provide useful insights into future possible paths to advancing current available tumor boundary delineation approaches to achieve efficacious tumor therapy.

*Corresponding author.
E-mail address: aiguo@nimte.ac.cn (Aiguo Wu).
[†]These authors made equal contributions to this work.

Peer review under responsibility of Chinese Pharmaceutical Association and Institute of Materia Medica, Chinese Academy of Medical Sciences.

https://doi.org/10.1016/j.apsb.2022.02.016

1. Introduction

Chemotherapy is a major clinically relevant strategy for cancer treatment, often preceding surgery and complemented with radiotherapy. Accurately mapping the boundaries of tumor tissues with surrounding healthy tissues are important for various therapeutic strategies, such as chemotherapy, radiotherapy and tumor resection. In the past years, various bioimaging modalities have been deployed to locate tumor tissues and form contrasts between tumor and healthy tissues. Some of such imaging modalities require the pre-injection of dye molecules and/or contrast agents that are usually not selective in action. It has also been observed that the imaging agents that are even administered intratumorally find their ways to neighboring tissues, thus jeopardizing effective tumor mapping. Additionally, low signal resolution of many available imaging modalities precludes them for use in proper tumor mapping. It is therefore desirable to develop a robust approach to map tumor boundaries with normal tissues. The gains of accurate tumor boundary mapping go beyond early diagnosis of tumor in clinic to enhancing adequate evaluation of tumor therapeutic outcomes, which hitherto pose serious challenges in both microscopic and macroscopic bioimaging techniques[1,2].

Present-day clinical tumor resection relies mainly on visual observations of the surgeon which is limited by human eye impairment and experience of the surgeon, particularly when the tumors are infiltrated and visually indistinguishable from adjacent normal tissues[3–5]. Complementary bioimaging with techniques such as magnetic resonance imaging (MRI) and fluorescence imaging have been leveraged to acquire information on tumor location to aid surgeons. However, intraoperative MRI has received less attention because it interrupts the surgical procedure and is expensive[6]. Fluorescence imaging on the other hand has garnered increasing interest as a rapid and cost-effective modality that locates tumor tissues by spectral properties during intraoperative tumor mapping, but suffers from relatively low spatial resolution[7,8]. Moreover, there are mounting reports on the toxic effects of MRI and fluorescence imaging contrast agents which complicate the reliefs that patients should experience after successful tumor treatment[9].

There have been concerted efforts by numerous researchers to detect the boundaries between tumors and normal cells. As a paradigm, single-point spectral measurements were utilized to develop a fluorescence imaging-based model for tumor boundary mapping to enhance intraoperative tumor resection[3]. It entailed a theoretical model obtained from observations of envisaged spectral signature when an excitation laser moves across a tumor boundary. Information from discretized contributions of established spectral signatures, including those from tumor and normal cells, were obtained in the tissue surface vicinity of the laser spot to derive the model, which enabled an enhanced tumor boundary detection irrespective of the disparity between laser spot size and target detection resolution.

In this review, we summarized the research advances in mapping tumor boundaries. First, we discussed the various techniques that have been applied to detect the boundaries. This was narrowed down to specific chemotherapeutic nanomaterials that have been synthesized in our research group in the past decade and their possible contributions to tumor boundary delineation. Second, a detailed look into the various tumors that have been investigated in this regard is provided. Finally, a perspective on the current status and prospects of adequately mapping tumor boundaries is presented. This study is therefore expected to provide meaningful guide for understanding the gains of proper boundary mapping between tumors and normal cells which can be leveraged to enhance current tumor therapeutic techniques, particularly chemotherapy.

2. Chemotherapeutic nanomaterials

The past decade has witnessed significant advances in nanomaterial-based drug delivery, especially for tumor treatment[10–13]. As regards tumor chemotherapy in general, research in our laboratories on tumor-targeted chemotherapeutic nanomaterials have also contributed a great deal to recent advances on tumor chemotherapy. Specifically, interesting nanomaterial-based drug delivery systems with excellent biocompatibility and tumor microenvironment responsiveness have been developed in our research group including doxorubicin (DOX)-loaded zeolitic imidazole framework (ZIF) nanomaterials with pH-responsiveness[14], cisplatin-loaded ZIF nanomaterials with mitochondrial targeting in platinum-resistant ovarian tumor[15], and 5-fuorouracil-loaded amorphous ZIF nanomaterials with high drug-loading and tumor microenvironment responsiveness[16]. Such nanomaterials demonstrated appreciable capability to deliver substantial amounts of chemotherapeutic drugs to tumor sites for achieving meaningful tumor regression.

Research on chemotherapeutic nanomaterials these days does not only involve using the nanomaterials for tumor chemotherapy, but also encompasses meaningful efforts to use chemotherapeutics as agents to enhance the efficacy and accuracy of tumor boundary delineation with fluorescence, MRI, CT, ultrasound, and other imaging modalities. The boundaries of various kinds of tumor cells including brain, liver, breast and prostate tumor cells have been delineated successfully in conjunction with chemotherapy, where drug delivery systems were used in a double-edge-sword approach to convey both chemotherapeutic drugs and bioimaging agents to tumor sites. Unfortunately, the toxicity and non-specificity concerns of typical chemotherapeutic nanomaterials coupled with the potential downsides of the degradation products of drug and bioimaging agents' combination in a single nanomaterial hitherto preclude wide adaptation of this approach. To the best of our information, nanomaterials that integrate both chemotherapeutic drugs and imaging agents are still in the pilot scale. Even though there are have been success in this approach, we believe that much effort is still needed to appropriately leverage chemotherapeutic nanomaterials for tumor boundary delineation and meet the stringent demands for clinical translation. The next section describes the use of chemotherapeutic nanomaterials in boosting tumor boundary delineation using various bioimaging modalities independently or in combinations.

3. Strategies for tumor boundary delineation

Early and accurate delineation of tumor boundary are key aspects in predicting patient survival rates and evaluating tumor microenvironment responses to radiation therapy and chemotherapy in both preclinical and clinical settings. In clinical aspect of tumor therapy also, accurately identifying invasive tumor edges of primary tumors, small tumor lesion that have been locally invaded, and drug-resistant tumors that remain after neoadjuvant therapy could substantially decrease the incidence of tumor recurrence and enhance survival rates of patients. Presently, gross examination

and frozen tissue section, as well as histological assessment of excised tumor dominate the landscape of clinical protocols for evaluating tumor boundaries[17,18]. However, such assessments are unreliable as the pathological evaluation of tumor tissues reveal high proportions of tissues with positive tumor boundaries[19,20].

The main drawback of accurate tumor boundary detection lies on non-invasive tumor lesions, which do not commonly exhibit clear-cut tumor boundaries[21]. Also, small distant tumors that localize around normal tissues also jeopardize accurate tumor boundary detection[17]. Inflammatory anomalies and fibrosis related to tumor-triggered obstruction or preoperative chemotherapy pose serious challenges to surgeons in determining tumor boundaries[22]. Moreover, just a hand full of frozen tissue sections can actually be evaluated in the tumor vicinity, which encourages the possibility of underrepresenting the involvement of tumor in the boundaries[23]. Based on the foregoing, more sensitive and accurate strategies have been explored for early and accurate detection of tumor boundaries. In the following sections, we discuss such strategies including fluorescence imaging, MRI, models and algorithms, and multimodal imaging.

3.1. *Fluorescence imaging*

Recent progress in developing molecular imaging contrast agents has enabled proper visualization of tumor boundaries by non-invasive optical imaging strategy. Various compounds including anti-cancer drugs, antibodies, peptides, and small molecules have effectively been labelled with optical imaging dyes to generate promising fluorescent probes[24–27].

Tumor boundary was adequately mapped by NIR fluorescence-labeled antibody[28]. The NIR antibody molecule was designed to target epithelial cell adhesion molecule which was validated by far red reporter iRFP expressed by the tumor cells. This enabled effective colocalization of the NIR molecule signals for direct evaluation of the tumor boundary (Fig. 1A). Receiver operating characteristic assessment was employed to validate the fluorescence signals against established pathology of local and metastatic tumor lesions, resulting in about 96% accuracy. Expectedly, the local tumor boundary was mapped with more accuracy using quantitative NIR fluorescence imaging with the epithelial cell adhesion molecule-targeting antibody in comparison with an isotope-labeled NIR antibody as control. This therefore established the potential of fluorescence imaging in accurately mapping tumor boundaries. However, there are some limitations in the study. For instance, the authors carried out *ex vivo* and *in situ* imaging as the mice small retroperitoneal cavity tissues were quite difficult for the clinical devices deployed in the study to access. Additionally, the metastatic prostate cancer model, a popular subcutaneous model, may not be significantly relevant in the clinic for delivering macromolecular fluorescence probes such as the NIR fluorescence-labeled antibody probe developed in the study.

Leveraging tumor-targeting, a urokinase plasminogen activator receptor-targeted probe was developed for effective fluorescent imaging of tumor boundary and chemotherapy[29]. This was achieved with the amino terminal fragment (ATF) of urokinase plasminogen activator in two systems: (1) near infrared fluorescence (NIR) dye-labeled recombinant 135-amino acid peptides, and (2) NIR-dye-ATF peptides conjugated to polymer-coated iron oxide nanoparticles. For more clarity, urokinase plasminogen activator is a serine protease that interacts with its corresponding receptor (urokinase plasminogen activator receptor) for the main purpose of regulating diverse pathways that occur in matrix degradation, metastasis, angiogenesis, and cell motility[30]. The nanoprobes accumulated in tumors, especially in tumor boundaries where they showed strong fluorescence signals. This enabled appropriate mapping of the tumor boundaries (Fig. 1B). It could be seen that strong signal for Cy5.5 and IRdye-800 were found in the tumor xenograft. Cy5.5 signal was also detected in the intestine region. Also, strong IRDye 800 signal was detected both in the tumor and liver tissues. A high magnification image of the tumor (zoom, 0.8 ×) showed the presence of Cy5.5-hATF probes (red fluorescence) in both the tumor center and the tumor border. However, the authors reported that a high amount of IRDye 800 ScFvEGFR probes (green fluorescence) was found in the center of the tumor. Moreover, the tumor-targeted chemotherapeutic nanomaterials enabled orthotopic MCF-10DCIS human breast and MIA PaCa-2 human pancreatic tumor chemotherapy by substantial DOX release from the nanocarrier system.

Impressive efforts have also been made in our research group to delineate tumor boundaries with nanomaterial-based drug delivery systems. This encompasses several researches where chemotherapeutic nanomaterials could also provide single or multimodal imaging of tumor for boundary delineation. As a paradigm, various nanocarriers have been developed in our laboratories and loaded with specific anti-cancer drugs that possess fluorescence imaging capability. For instance, change in membrane protein as a result of multidrug resistance by cancer cells (MCF-7/ADR)[31], was leveraged to develop a promising chemotherapeutic cancer treatment strategy in our research group[32]. As Y_1 receptor protein and P-glycoprotein are overexpressed on multidrug resistant cancer cells, a selective Y_1 ligand (AP) was deployed to stabilize an anti-cancer drug (DOX) and P-glycoprotein inhibitor tariquidar (Tar) co-loaded nano-micelles (Fig. 2A). The co-delivered P-glycoprotein inhibitor tariquidar successfully impeded DOX efflux with resultant enhanced targeted drug delivery and accumulation in multidrug resistant cancer cell nuclei to significantly inhibit cancer cell proliferation. It is also of interest to note that this strategy prevented liver metastasis, a common occurrence in cancer cases responsible for numerous cancer-related deaths, resulting in prolonged survival extents up to 60 days post-treatment (Fig. 2B). More importantly, a near infrared Dye moiety (IRDye 780) was incorporated into the nanomicelle which enabled adequate determination of tumor boundary by fluorescence imaging (Fig. 2C), which could provide useful information on the size and boundary of tumors during treatment monitoring.

A facile green strategy was used to develop DOX-loaded nanoparticles which afforded tumor chemotherapy on the one hand and enabled fluorescence imaging mapping of breast tumor boundary on the other hand[33]. The nanoparticles of 70 nm size and surface charge of −20 mV was also loaded with a photosensitizer (chlorine e6, Ce6) to achieve photodynamic tumor therapy and complement the chemotherapeutic outcomes. The loaded DOX and Ce6 could effectively reach tumor sites because they were linked by electrostatic, $\pi-\pi$ stacking and hydrophobic interactions. Moreover, the size of the nanoparticles enabled their penetration of tumor cells by the enhanced permeability effect (passive tumor targeting) where a one-cycle treatment resulted in no tumor recurrence attributed to the synergetic treatment strategy. In another study, a chemotherapeutic nanomaterial was engineered and loaded with the anti-cancer drug mitoxantrone[34]. Fluorescence imaging of lung tumor in mice resulted in effective delineation of the tumor boundaries, where real-time evaluation of drug dispersion in the tumor was also achieved.

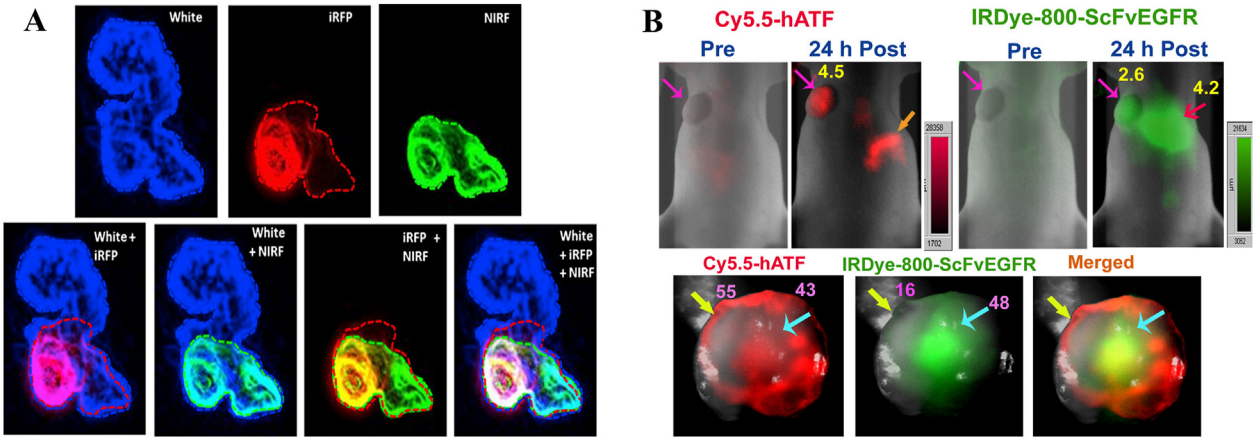

Figure 1 (A) The boundaries of a representative local tumor lesion as obtained by boundary analyses of white light, NIRF signals, iRFP, and their corresponding overlays. The boundaries codenamed by iRFP threshold which were determined by ROC analyses and NIRF contrast of 1.86 are indicated on the image. Adapted with permission from Ref. 28. Copyright©2013, World Molecular Imaging Society. (B) Simultaneous imaging of urokinase plasminogen activator receptor and EGFR expression in a human breast cancer xenograft using NIR-dye labeled ATF and ScFvEGFR peptide probes. Nude mouse bearing an orthotopic MDA-MB-231 human breast cancer xenograft received a tail vein delivery of a mixture of 50 μg of Cy5.5-human ATF and 50 μg of IRDye 800-ScFvEGFR for 24 h. Numbers shown in the images are signal to body background ratios. Adapted with permission from Ref. 29. Copyright©2013, Ivyspring International Publisher.

3.2. MRI

Tumor imaging by MRI could provide information on tumor location but subtle changes in tumors may be quite difficult to notice[35,36]. Even though radiologist have over time traced tumor boundaries manually in a bid to roughly estimate tumor sizes, this practice is time-consuming and tedious. Therefore, routinely applying this process would be impractical and the results may be inconsistent and unreproducible due to significant intra- and inter-observer differences. In this paradigm, Law et al.[37] presented an approach to extract brain tumor boundary in two-dimensional (2D) MR images. In each image slice, the initial plan used was extracted from the boundary of the preceding image slice. The tumor boundaries were then mapped by region and contour deformation. This method is advantageous as it has the capability of tolerating rough initial plans. Moreover, only one coarse initial plan is required for all other MR image slices in the series. The authors therefore utilized information from tumors in consecutive MR images to

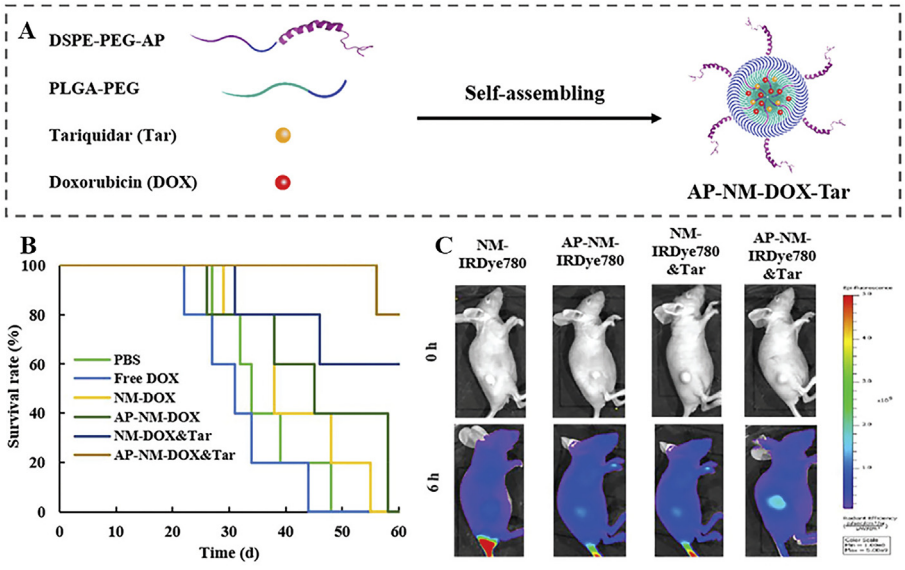

Figure 2 (A) The preparation of Y_1 receptor ligand-functionalized chemo drug DOX and P-glycoprotein inhibitor tariquidar (Tar) coloaded nanomicelles. (B) Survival extents of mice after tail vein injection of different micelles. (C) *In vivo* fluorescence imaging of tumor-bearing mice before and after the intravenous injection of NM-IRDye780, AP-NM-IRDye780, NM-IRDye780&Tar, and AP-NM-IRDye780&Tar at 6 h (IRDye780: 0.25 mg/kg). Adapted with permission from Ref. 32. Copyright©2019, Royal Society of Chemistry.

evaluate the potency of the approach on MR image set. They found that the approach they used could map tumor boundaries in MR images more effectively than by manual tracing.

MRI also plays a crucial role in neurosurgery by providing adequate image guidance, and can potentially map the boundaries of residual glioma after the first surgery and provide update on neuronavigation data which compensates for brain shift resulting from loss of cerebrospinal fluid and the removal of brain tissue[38]. However, it was reported that intraoperative magnetic resonance spectroscopy could substantially assist in mapping the biological boundaries of gliomas[39].

Research in our laboratories involving nano-ZIF-90 drug delivery system combined Y_1 receptor protein overexpression in tumors with Mn and 5-fluorouracil loading to obtain a tumor chemotherapeutic nanomaterial with potential for delineating tumor boundary by MRI (Fig. 3A)[40]. The nano-ZIF-90 was post-synthetically modified with a specific Y_1 receptor [Asn[28], Pro[30], Trp[32]]-NPY (APT). The nano-ZIF system exhibited dual targetability for breast cancer and mitochondria, appreciable biocompatibility, minimal 5-fluorouracil erosion during *in vivo* circulation, and ultimate substantial tumor regression in a typical targeted tumor chemotherapy. Of course, the Mn moiety is responsible for the T_1-weighted MRI signal enhancement in the tumor region (Fig. 3B), thus providing insights into the exact location, size and boundary of tumor that could benefit successful tumor resection in the clinic.

Taking the interaction of chemotherapeutic nanomaterials with macrophages *in vivo* into account, our research group developed a Y_1 ligand (AP)-functionalized biodegradable photoluminescent waterborne polyurethane (BPLP-WPU) polymeric nano-micelles (denoted as BWM) with antiphagocytosis capability for tumor chemotherapy[41]. The was successfully imparted on the nano-micelles by incorporating a self-peptide (SP) designed from CD47 human glycoprotein. The nano-micelle also featured DOX and superparamagnetic iron oxide nanoparticles (SPION) co-loading to achieve tumor chemotherapy and MRI-enabled adequate detection of tumor, respectively. Upon intravenous injection of the nano-micelles, the Y_1 ligand promoted targeting of tumor cells, where DOX was substantially released *via* pH responsiveness (Fig. 3C). This strategy significantly reduced drug leakage during circulation, thus minimizing chemotherapeutic drug-associated side effects (toxicity), prolonging survival times, and ensuring that sufficient quantity of drugs is conveyed to the tumor site to achieve efficacious treatment. Moreover, the co-loaded SPION in the AP&SP-BWM-SPION afforded T_2-weighted MRI signal enhancement in the tumor region in furtherance of adequate tumor location, size determination, and boundary delineation (Fig. 3D).

Chemokine (C-X-C motif) receptor 4 (CXCR4), overexpressed in esophageal cancer cells, was utilized in recent research in our laboratories to synthesize a nano-ZIF-7 drug delivery system for tumor chemotherapy[42]. Different from regular tandem nano-assemblies[43], the study is the first report on tandem post-synthetic modification of ZIF-7 by exchanging the ZIF-7 network with an organic ligand (CXCR4 inhibitor) and Mn ions. This strategy yielded an active-targeting nano-ZIF-7 network with capacity for 5-fluorouracil loading to effect DNA damage in esophageal cancer cells. Advantageously, the Mn ions provided the much-desired T_1-weighted MRI signal enhancement in the tumor region, which not only guided the tumor chemotherapeutic strategy but provided useful information on the size and boundary of the tumor.

In addition to delineating tumor boundary, another study went a step further to also use MRI to monitor the spatial and temporal DOX-release patterns in rats bearing 12 mm fibrosarcoma[44]. The nanomaterial described in the study had lysolipid-based temperature-sensitive liposomes as the DOX carrier and manganese as the MRI contrast agent. The researchers also deployed Kruskal−Walli's test and the Kaplan−Meier product-limit method to determine DOX concentration in tumors and tumor volume variations. Importantly also, the study established that hyperthermia is responsible for the release of DOX and manganese from the temperature-sensitive liposomes at the tumor sites for chemotherapy and clear-cut MRI-guided tumor boundary mapping, respectively. In another study, the boundary of bladder tumor, a common urinary tract tumor in the clinic, was effectively delineated by MRI using vincristine-loaded polydopamine-coated Fe_3O_4 nanoparticles[45]. Polydopamine, a conductive polymer, in the chemotherapeutic nanomaterial was leveraged to offer tumor photothermal therapy to complement vincristine-mediated chemotherapy, while the common MRI contrast agent Fe_3O_4 nanoparticles offered MRI-guided tumor boundary delineation. Another chemotherapeutic DOX-loaded nanomaterial enabled clear delineation of tumor boundary when a pH-switching MRI agent based on manganese was successfully delivered to the tumor site alongside the chemotherapeutic DOX[46]. Both positive and negative MRI contrast enhancements in the tumor region were recorded as pH changed. Specifically, relaxivity changed from 0.65 to 5.61 L/(mmol·s) as pH decreased from 7.4 to 4.5. At the same time, the DOX moiety in the nanomaterial which could provide effective tumor regression was released progressively as manganese ions were released from the chemotherapeutic nanomaterial. It then follows that the nano-delivery system described in the study is capable of progressively releasing both DOX and manganese ions to offer simultaneously tumor regression that could be monitored from its delineated boundary.

3.3. *Ultrasound imaging*

The major advantages of using ultrasound in the clinic for tumor detection are that the ultrasound equipment is relatively cheap and convenient. Notwithstanding, there are literature reports that suggest that intraoperative ultrasound is not actually ideal for detecting tumor residues[47,48]. A group of researchers have also pointed out its susceptibility to peritumoral edema, hemorrhage, and other interference causes[49]. The good news is that advancements in ultrasound technology, heralding the development of linear array ultrasound and 3D ultrasound have significantly enhanced the quality of intraoperative ultrasound images[50,51]. Also, B-mode ultrasound technique holds the promise of improving the extent of tumor resection and patient prognosis, especially for brain tumors but still have some challenges in tumor boundary delineation as biopsies reveal tumor cells beyond the boundaries mapped by such technique[52].

In as much as the B-mode ultrasound has been deployed in mapping tumor boundaries and can offer comparable accuracy in residual tumor detection as with intraoperative MRI[53], it cannot effectively delineate biological tumor boundaries. As the technique could identify blood vessels, cortical structures, co-register multi-modal preoperative ultrasound images, and correct surgical resection-triggered tissue deformation[54], it may be possible to accurately delineate tumor boundary by the preoperative multi-modal ultrasound images. The authors in this review therefore

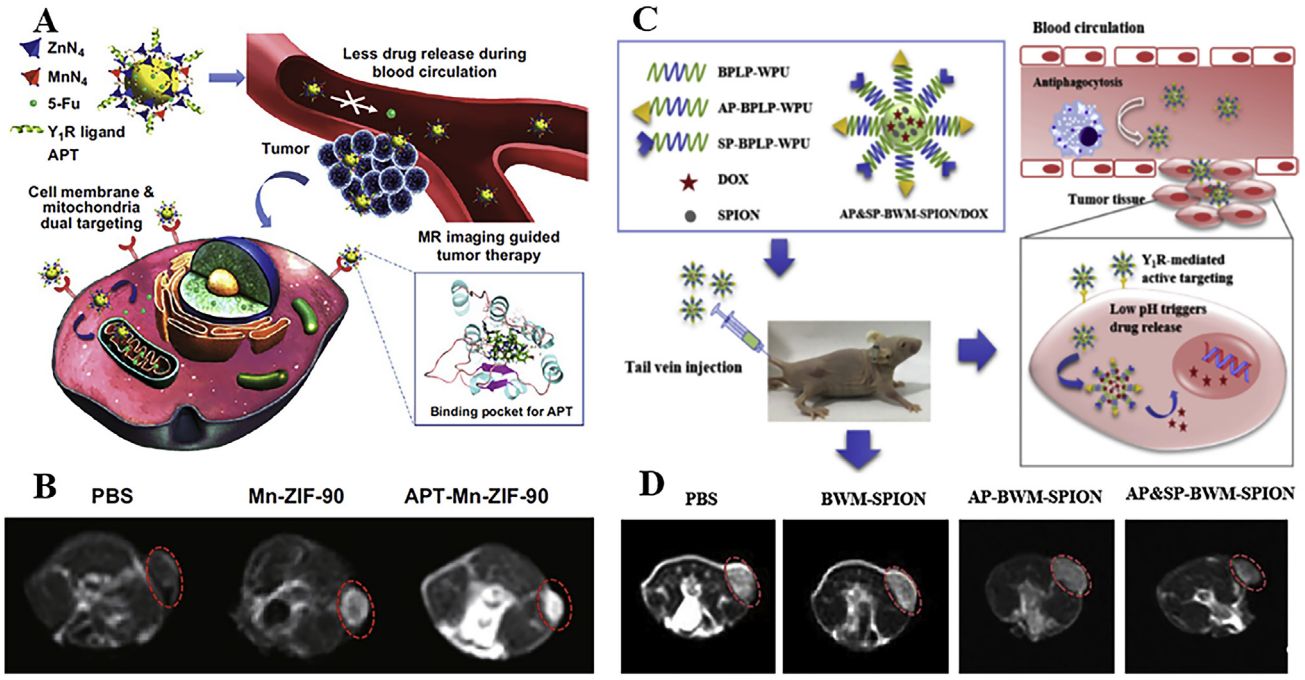

Figure 3 (A) Schematic of bio-application and potential mechanism of APT-Mn-ZIF-90/5-Fu for tumor therapy and the binding mode of APT with Y_1R. The binding mode of APT with Y1R is shown on the lower right side; Y_1R is shown in cartoon representation. APT (green carbons) and receptor residues (pink carbons) involved in the ligand binding are shown as sticks. The H-bonds are represented by the yellow dashed lines. (B) T_1-weighted MR images of MCF-7 tumor-bearing nude mice after intravenous injection of PBS, Mn-ZIF-90, and APT-Mn-ZIF-90 at 24 h, the red circles indicate the tumor regions. Adapted with permission from Ref. 40. Copyright©2019, Creative Commons Attribution License. (C) Y_1 receptor ligand (AP) and SP-functionalized novel BPLP-WPU micelles (BWM) could evade premature drug erosion and macrophage opsonization during systemic circulation. (D) *In vivo* T_2-weighted MR images of MCF-7 tumor bearing nude mice 20 h after intravenous injection of AP&SP-BWM-SPION (15 mg/kg for Fe). Adapted with permission from Ref. 41. Copyright©2018, Elsevier Limited.

believe that the actual advantage of intraoperative B-mode ultrasound is in providing real-time imaging guidance during tumor treatment. Notwithstanding, chemotherapy has enabled effective breast tumor boundary delineation with B-mode ultrasound imaging[55]. The shape parameter of integrated backscatter and homodyned K distribution, as well as tumor size in the longest measured dimension, were successfully assessed based on B-mode ultrasound information which also served as a marker for neoadjuvant chemotherapeutic response. This strategy was then successfully deployed in a recent study to effectively delineate breast cancer boundaries prior to neoadjuvant chemotherapy[56].

B-mode ultrasound has been used to clearly map the boundary of breast tumor in mice with the aid of a chemotherapeutic nanomaterial[57]. The study used a mixture of DOX-encapsulated polymeric nanoparticles and perfluoropentane (PFP) nano/microbubbles that were stabilized by the same biodegradable block copolymer to achieve the tumor chemotherapy and boundary delineation. When intravenously injected into mice, the DOX-encapsulated polymeric nanoparticles and PFP nanobubbles preferentially extravasated into the interstitium of tumors. Consequently, the nanobubbles could coalesce to generate microbubbles with strong, long-lasting ultrasound contrast that effectively delineated tumor boundaries. Additionally, the DOX was significantly retained within the microbubble cavity but released on-demand in response to therapeutic ultrasound. In a more elaborate chemotherapeutic nanomaterial design *via* film dispersion method, liposome was used as a nano-carrier to encapsulate DOX, gold nanospheres, and PFP for tumor photothermal-chemotherapy and ultrasound imaging[58]. Whereas gasification of the PFP enabled ultrasound-mediated tumor boundary delineation (Fig. 4), the gold nanospheres converted near infrared light to heat to afford tumor photothermally reinforced chemotherapy mediated by DOX.

3.4. *Mammography*

Mammography is a standard method for early identification of tumor cells. It is however impractical for radiologists to analyze numerous mammogram images per day as it could be tedious and time-consuming, which could cause false positives or false negatives. Typical mammogram images usually have labels, scratches, and pectoral muscles, which are quite difficult to expound. Such artefacts possess dense grey values that appear as abnormal images, which could misguide presenting segmentation strategies and hinder segment accurate pathology-bearing regions. Therefore, it is important to suppress the artefacts to improve the reliability of mammography, especially for biomedical application[59,60]. Also, as the visual appearance of mammogram images are quite indistinguishable, proper delineation of tumor boundaries in such images is crucial in computer-aided diagnosis (CAD) systems[61]. Early studies showed that mammography has also been used to screen asymptomatic women to enable the detection of occult breast cancers and to minimize mortality rates by 30% in women (50–69 years)[23,29].

In biomedicine, mammography has been successfully deployed in various imaging aspects for delineation purpose. For instance, Mustra and Grgic[62] presented an adaptive contrast enhancement protocol to detect breast skin-air interface in a typical CAD

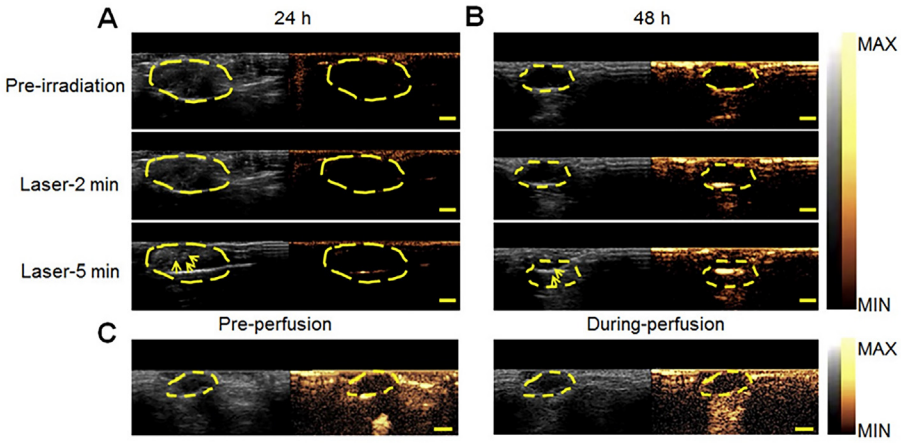

Figure 4 *In vivo* ultrasound images of tumor sites in 4T1 tumor-bearing mice at 24 h (A) or 48 h (B) post-injection of DHPL-29. The tumor sites were treated with NIR laser irradiation (2 W/cm^2) for 2 min or 5 min. (C) *In vivo* ultrasound images of tumor sites in 4T1 tumor-bearing mice before and during the perfusion of SonoVue®. The yellow dotted line indicates tumor sites. The yellow arrow indicates microbubbles produced after NIR light irradiation. Scale bars, 0.5 cm. Adapted with permission from Ref. 58. Copyright©2018, Ivyspring International Publisher.

system. The protocol combined adaptive histogram equalization strategy on a small are of interest that contained actual edge and edge detection operators. They also delineated pectoral muscle by combining contrast enhancement utilizing adaptive histogram equalization and polynomial curvature estimation on selected area of interest. Recently, Zebari et al.[63] used mammography to delineate the breast region in mammogram images obtained from image analysis society (mini-MIAS), INbreast, and Breast Cancer Digital Repository (BCDR) databases, which informed the boundary of breast and pectoral muscle for proper breast tumor detection during treatment monitoring.

Nanomaterials have also found their way into mammography imaging and subsequent tumor boundary delineation. For instance, gold nanoparticles were recently investigated for mammographic molecular imaging and showed very promising performance[64]. Notably, optimized conditions of nanoparticle size (10−20 nm) and injection concentration (10 mg/mL or higher) were established in the study to guide future development of nanomaterials for mammographic imaging. Breast tumor boundary delineation with the gold nanoparticles enabled an estimation of the tumor size (Fig. 5A−D). Hsu et al.[65] in another recent study on the utilization of nanomaterials in mammography showcased silver-sulfide nanoparticles with size-tunability property for dual-energy mammography. Renal clearance of silver-sulfide nanoparticles has been a limitation to their clinical translation for use in other bioimaging modalities such as CT and fluorescence imaging where such nanoparticles have been found effective[66,67]. It is interesting to note that the 3.1 nm silver-sulfide nanoparticles synthesized by Hsu et al.[65] are renally clearable as about 85% of the injected dose was cleared *via* urine in 24 h post-injection. These recent successes in utilizing gold and silver-sulfide nanoparticles in mammographic imaging suggest that chemotherapeutic nanomaterials could also be introduced to achieve simultaneous tumor chemotherapy and boundary delineation.

3.5. *Raman imaging*

Raman spectroscopy detects inelastic scattered light emanating from the interaction of matter and light[39]. It therefore provides information on the chemical fingerprints of cells, biological fluids and tissues. It can effectively differentiate between white matter, gray matter, necrosis, and glioma, which positions it as a potent technique for intraoperative identification of residual tumors[68]. Using a portable handheld device in direct contact with the tumor resection boundary, Raman spectroscopy can intraoperatively identify tumors which are unidentifiable with MRI[69]. Consequently, numerous Raman spectroscopy modalities have been developed such as surface-enhanced Raman scattering[70,71], surface-enhanced resonant Raman spectroscopy[72,73], stimulated Raman spectroscopy (SRS)[74,75], and coherent anti-Stokes Raman spectroscopy (CARS)[76,77], which have been shown to play significant roles in identifying glioma boundaries[78].

Compared with other label-free bioimaging methods (*e.g.*, two-photon fluorescence, second harmonic generation, and third harmonic generation)[22], coherent Raman spectroscopy including SRS and CARS have high chemical selectivity, which enable their application in complex bioimaging procedures such as brain imaging[79,80]. Particularly, SRS and CARS provide improved sensitivity against conventional Raman scattering because of the coherence of their signal production, which enables fast and real-time imaging in epi-mode or reflectance[81,82]. The inherent 3D optical sectioning ability of nonlinear optical spectroscopy is suitable for intraoperative bioimaging, which eliminates the necessity of thin tissue sectioning for creating microscopic images[83]. Furthermore, SRS microscopy offers the unique advantage of rapid histopathological analysis *in situ* against traditional histopathology. It also outperforms CARS in bioimaging due to its inherent linear relationship between signal intensity and chemical concentration, and non-distorted spectrum which has close resemblance with spontaneous Raman spectrum, consequently allowing for quantifying chemical imaging[84].

Nanomaterials have also been integrated with SERS imaging and therapeutic modalities including chemotherapy, photothermal therapy, and photodynamic therapy[85,86]. A recent smart design of chemotherapeutic nanomaterial with SERS imaging capability that effectively mapped tumor boundaries and evaluated drug scattering in tumors alongside cellular imaging has been reported[34]. The study also enabled real-time monitoring of anti-cancer mitoxantrone drug release throughout cell cycle in a low-dose (200 μg/mL) chemotherapy. SERS spectra of three different tumors were also

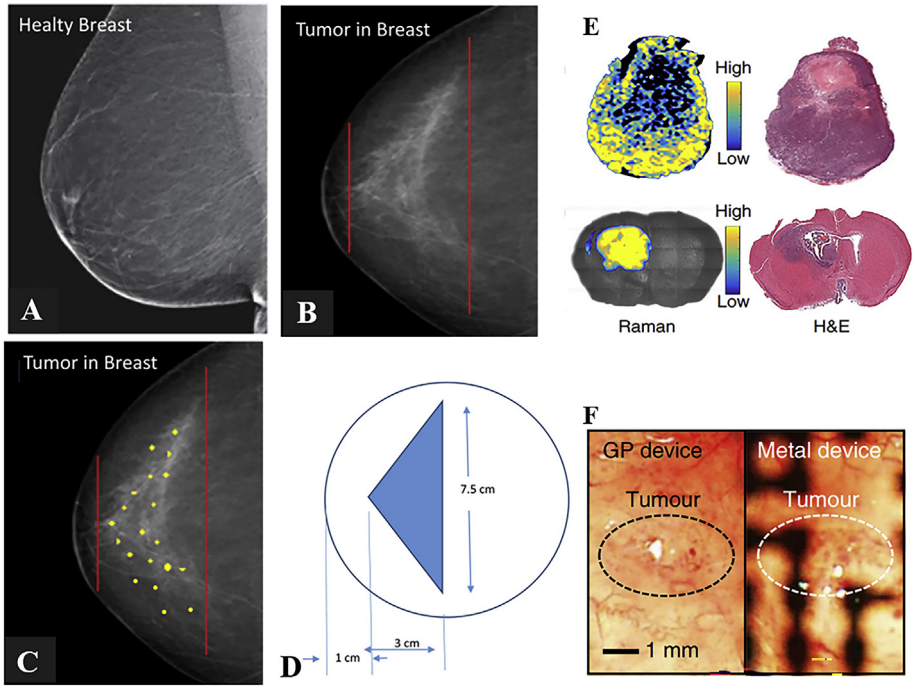

Figure 5 Mammogram image of the healthy breast (A), the breast with calcified tumor (B), the image schematizes the insertion of Au-NPs in the tumor tissue (C) and the geometrical dimension of the tumor volume (D). Adapted with permission from Ref. 64. Copyright©2019, Elsevier Limited. (E) *Ex vivo* Raman images of excised ovarian tumor and glioblastoma mouse brain tumor with adjacent H&E histology correlation. Adapted with permission from Ref. 90. Copyright©2019, Creative Commons Attribution License. (F) Tumor images captured by the camera of the endoscope through electronic devices (left: through transparent bioelectronic devices; right: through control metal devices) after chemotherapeutic nanomaterial administration. Adapted with permission from Ref. 101. Copyright©2015, Creative Commons Attribution License.

successfully obtained using the chemotherapeutic nanomaterial, thus pointing to the effectiveness of SERS imaging in a variety of tumors and their boundary delineation. Also, the *in vivo* SERS detection of the chemotherapeutic nanomaterial holds strong promise for SERS image-guided cancer chemotherapy. Hu et al.[87] also deployed SERS detection in their report of docetaxel-mediated tumor chemotherapy. Whereas SERS imaging enabled clear-cut detection of the tumor, the anti-cancer drug (docetaxel) provided chemotherapy using the rod-shaped chemotherapeutic nanomaterials with average size between 40 and 120 nm. Another study investigated pH-triggered chemotherapy combined with photodynamic therapy and SERS imaging with a chemotherapeutic nanomaterial[88]. The design strategy of the spherical 70-nm silver nanoparticles-based chemotherapeutic nanomaterial features decoration with folic acid targeting ligand by amide bond linkage, and conjugation to DOX by acid-cleavable hydrazone bond. A polyethylene oxide spacer was used to attach the folic acid to DOX for ensuring plethora delivery of DOX to tumor cells *via* folate-mediated endocytosis. Subsequently, SERS detection of the tumor cells was possible, aided by the chemotherapeutic SERS nanobioprobe.

He et al.[89] demonstrated a smart design of Raman tagged core-shell chemotherapeutic nanomaterials which simultaneously performed tumor chemotherapy, phototherapy, and SERS imaging. The nanomaterial (denoted as $Au@Cu_3(BTC)_2$) specifically comprised of gold nanoparticles (core), 4-mercaptobenzoic acid (Raman reporter molecule), DOX (chemotherapeutic agent), and copper(II) carboxylate metal organic frameworks (shell). Not only did the gold nanoparticles core act as a photothermal agent to thermally destroy tumor cells and promote DOX release for chemotherapy, it also served as a SERS substrate to enhance the Raman signal of 4-mercaptobenzoic acid. Subsequently, it was clear to distinguish the boundaries of A549 cells by the chemotherapeutic nanomaterial-mediated SERS mapping. Raman imaging modality was also used in a recent study to delineate breast tumor and glioblastoma brain tumor boundaries in mice model using DNA-decorated gold nanoparticles (Fig. 5E)[90]. Even though no chemotherapeutic drug was loaded in the nanomaterial, the effectiveness of DNA-decorated gold nanoparticles in the imaging suggests that chemotherapeutic nanomaterials can also be integrated to even enhance the gold nanoparticles-mediated photothermal therapeutic performance alongside tumor boundary mapping.

Also, SERS mapping of tumor boundary was possible with the DOX component of a chemotherapeutic nanomaterial[91]. In the two-step SERS mapping, both DOX and graphene oxide nanoparticles could be effectively traced to give clear-cut boundary regions of the tumors, where DOX component provided pH-responsive tumor chemotherapy that was complemented by gold nanoparticles-mediated photothermal therapy. From the foregoing, we infer that reports on effective tumor boundary delineation with chemotherapeutic nanomaterials *via* SERS imaging are still scarce but could be a promising strategy.

3.6. *Endoscopy*

Recent advancements in endoscopy including narrow band endoscopy and magnified endoscopy have yielded improved possibilities of tumor boundary delineation. Boundary delineation by image-enhanced endoscopy is by digital endoscopy, optical

digital endoscopy, and chromoendoscopy. Digital endoscopy involves setting a particular wavelength of observation with consideration of traditional endoscopic images to process and improve the visualization of images[92–94]. Optical digital endoscopy requires an optimization of the central wavelength between 415 and 540 nm as light is intensively absorbed by blood and subsequently reflected at the gastric mucosa[95,96]. This method is particularly useful in acquiring clear images in the short-wavelength region. In chromoendoscopy-based delineation, three methods prevail: (1) contrast method where unevenness is achieved between tissues with indigo carmine or acetic acid, (2) staining method involving the use of toluidine blue to stain biological tissues of interest, (3) dye reaction method in which dyes such as Congo red undergo reactions to highlight specific tissues, and (4) fluorescence method where a fluorescent dye such as acridine orange is injected in the mucosa to observe fluorescence at select regions[97–100].

In this paradigm, Iizuka et al.[97] determined the lateral spread of gastric cancer lesion using a combination of indigo carmine and acetic acid method to provide useful tumor preoperative guidance. This strategy enabled a clear naked-eye observation of delineated gastric tumor boundaries in lesions. In a related study involving 104 gastric cancer patients, Kawahara et al.[98] early-stage gastric cancer was first observed in the patents and sprinkled with indigo carmine. The researchers used a graphic software to delineate boundaries of the early-stage gastric cancer which provided clear-cut visualization of the tumor boundaries.

As the gastrointestinal tract is quite difficult to access and target during tumor diagnosis and/or treatment, endoscopy that integrates imaging and treatment in the gastrointestinal tract are highly sought-after. This quest in endoscopy formed the basis of a report where a light from an endoscope was used to disassemble a nanocarrier, subsequently releasing the loaded chemotherapeutic drug DOX for both tumor treatment and boundary mapping purposes[101]. Interestingly, the strategy not only enabled tumor boundary mapping, but also provided temperature monitoring, pH sensing, radio frequency ablation, photothermal therapy and chemotherapy of colon tumor. However, tumor boundary delineation with the chemotherapeutic nanomaterial was not clear-cut (Fig. 5F). The study therefore points to a basis for closed-loop solution to colon tumor treatment. Endoscopy was also used for real-time imaging of chemotherapeutic SERS nanoparticles in the gastrointestinal tract[102]. The strategy enables multiplexed molecular data generation and quick circumferential scanning of the hollow organ surfaces such as the gastrointestinal tract to produce quantitative images of relative concentrations of the nanoparticles. Although the study did not involve tumor imaging and/or tumor boundary delineation, it strongly contributes to the application potential of nanoparticles in endoscopy-mediated imaging, which could be expanded to introduce chemotherapeutic nanomaterials.

3.7. *CT imaging*

The use of CT scanning to delineate tumor boundaries dates back to 1980s when Williams et al.[103] compared human observation of liver boundaries with their computer-edge detection algorithm. They tested computer program performance on lucite liver tumor phantom CT images. This included normal livers with computer-generated pseudo tumors of given size, liver tumor edge gradients, and object contrast, and 12 abnormal livers with 19 focal tumors, eight well-characterized and 11 ill-characterized tumors. The edge-linking algorithm successfully delineated the boundaries of pseudo tumors with object contrast of 3% or higher. In the abnormal livers, the algorithm successfully delineated nine focal tumors, provided near success in five focal tumors, but failed in five focal tumors. Generally, the performance of the algorithm is consistent with that of the human observer but was not recommended for routine clinical use.

Chemotherapeutic nanomaterials have been explored for tumor boundary delineation using CT scans. For instance, radionuclide technetium-99m labeled dendrimer-entrapped gold nanoparticles were synthesized for tumor imaging and loaded with DOX to also achieve breast tumor chemotherapy[104]. The researchers reported that the chemotherapeutic nanomaterials exhibit appreciable colloidal stability in various conditions, biocompatibility, and can be successfully labeled with the radionuclide with high radiochemical stability. However, the boundaries of breast tumors they investigated *in vivo* were not clearly delineated by the CT scanning. Keshavarz et al.[105] investigated a chemotherapeutic nanomaterial for CT imaging and cisplatin-mediated chemotherapy. They found that the alginate-based chemotherapeutic nanomaterial that was co-loaded with gold nanoparticles and cisplatin could substantially reduce the proliferation of CT26 cells derived from mouse colon adenocarcinoma, and provided CT contrast enhancement *in vitro*. Unfortunately, there were no *in vivo* investigations in the study to establish the *in vitro* results and test the tumor boundary delineation capability of the nanomaterials.

Another *in vitro* study used FePt chemotherapeutic nanomaterials to study CT imaging and chemotherapy of HeLa cells[106]. It was reported that the viability of cells significantly decreased after incubation with the FePt nanoparticles with an observed concentration-dependent CT signal enhancement. There are also no *in vivo* data to understand the behavior of the nanomaterials in animal models, especially for tumor boundary delineation. Zhu et al.[107] investigated dendrimer-entrapped gold nanoparticles that were loaded with the anti-cancer drug DOX for CT-guided chemotherapy. The chemotherapeutic agent featured gold core 2.8 nm, DOX moieties conjugated onto each of the dendrimers, and exhibit colloidal stability in various conditions. Although substantial DOX-induced and pH-responsive tumor-growth suppression and CT imaging of brain tumor, the study lacked *in vivo* data which could have provided information on tumor boundary delineation with the chemotherapeutic nanomaterials. From our literature search, we can infer that CT-based tumor boundary delineation with chemotherapeutic nanomaterials is quite scarce.

3.8. *Multimodal imaging*

Multimodal bioimaging leverages complementary information from a combination of imaging modalities to provide a more wholistic imaging of tissues. In a study that pathologically compared multitarget biopsy that was guided by multimodal bioimaging revealed that multimodal bioimaging can map tumor boundaries beyond what could be achieved with single imaging modalities such as MRI alone[108]. Moreover, various studies have buttressed this by establishing that multimodal imaging approach to tumor boundary delineation can improve the extent of resection and patient prognosis[39,109,110]. For brain tumor treatment, it was reported that when the treatment was guided by multimodal neuronavigation, tumors could be precisely located prior to craniotomy[111].

Zhou et al.[112] deployed both fluorescence spectroscopy and Resonance Raman spectroscopy to delineate tumor boundaries

relying on native molecular fingerprints of gastrointestinal and breast tissues. The approach leveraged the benefits of Resonance Raman spectroscopy *in situ* for diagnosing real-time tumor variations which provides a very useful modality for image-guided intraoperative boundary assessment in clinic, and could benefit postoperative evaluations. Using Resonance Raman spectroscopy, tumor boundary delineation was conducted by scanning lesion from the center or around the tumor area *ex vivo* for determining the variations in tumor tissues with normal tissue rims and considering native molecular fingerprints. Accurate tumor boundary delineation was recorded from the variations in Resonance Raman spectral peaks within a distance of 2 mm. The researchers verified the results with fluorescence spectroscopy conducted at excitation wavelengths of 300, 320, and 340 nm within a positive boundary, using normal tissues as reference. They therefore established a combination of dual modal (Resonance Raman spectroscopy and fluorescence spectroscopy) technique for accurate label-free tumor boundary delineation for intraoperative clinical evaluations.

In an early study involving 26 patients, MRI and CT imaging modalities were conducted to ascertain primary tumors in bone and soft tissues[113]. Both imaging modalities provided real-time detection of tumors. However, MRI technique effectively delineated the tumors and their relation to neighboring tissues in 21 out of the 26 patients. Not just the tumor delineation, MRI also provided superior visualization of marrow abnormalities in 12 patients than was attained with CT scanning. The researchers therefore recommended MRI over CT as the preferrable imaging modality for assessing and delineating tumors in bone and soft tissues.

Recent studies have also featured the application of nanomaterial-based drug delivery systems for potential multimodal tumor boundary delineation. Particularly, Fe(III)-complexed porous coordination network (PCN) was synthesized in nanometer size to detect tumor by both fluorescence imaging and MRI using a chemotherapeutic nanomaterial denoted as PCN-Fe(III)-PTX[114]. The complementarity of both imaging modalities is useful to enhance adequate size and boundary delineation of tumor. Fluorescence imaging-based determination of tumor area was a consequence of the tetrakis (4-carboxyphenyl)-porphine component of the chemotherapeutic nanomaterial, while T_1-weighted MRI signal enhancement was by the Fe moiety (Fig. 6A–C). Moreover, the nanomaterial provided sufficient release of an anti-cancer drug (paclitaxel, PTX) in tumor region and generated reactive oxygen species to afford chemo-photodynamic cancer therapy (Fig. 6D).

Ultrasound and photothermal imaging have also been combined in our research group to determine the location and boundary of tumor tissues in mice using a ZIF-90-based chemotherapeutic nanomaterial[115]. The nanomaterial was coated with polydopamine to imbibe it with photothermal therapeutic and imaging capabilities which complemented the DOX-mediated chemotherapy to achieve synergistic tumor treatment. Another study showcased the deployment of SERS and fluorescence imaging modalities in delineating tumor boundaries using a silver nanoparticles-based chemotherapeutic nanomaterial[88]. Interestingly, effective tumor regression mediated by the anti-cancer drug DOX and its biodistribution in tumor were adequately monitored by fluorescence imaging. Endoscopy was also combined with fluorescence imaging in a study with DOX-loaded chemotherapeutic nanomaterial to achieve tumor boundary delineation[101]. The researchers utilized active targeting *via* antibody conjugation to target colon tumors (HT-29) using the chemotherapeutic nanomaterial. Upon light irradiation from the endoscope, DOX was released to effect tumor chemotherapy, while its inherent fluorescence property was leveraged to image tumor and delineate corresponding boundaries by fluorescence imaging. The advantages and disadvantages of the various tumor boundary delineation strategies are summarized in Table 1.

4. Tumors types in boundary mapping

4.1. Brain tumor

Brain tumor is still one of the most difficult tumors to treat with nanomaterial-based drug delivery systems, due to the impedance of blood–brain barrier[126]. However, attempts have been made to adequately map the boundaries of brain tumors. For instance, Zhu and Yan[127] proposed a method for mapping brain tumor boundaries in MRI images using a Hopfield neural network. The boundary mapping problem was formulated *via* optimizing the boundary points to decrease energy functions based on active contour model. Impressively, the method offers less computing time against the 'snakes' algorithms, thus positioning it as a faster approach to mapping brain tumor boundaries. In another study, brain tumor segmentation was conducted using a set of preprocessing steps followed by morphological operations[128]. Models and algorithms have also been employed in delineating brain tumor boundaries in MRI images. For instance, Zhu and Yan[127] used a Hopfield neural network to delineate tumor boundaries in human MRI scans. Chan et al.[129] also utilized model and algorithm-based approach to successfully delineate brain tumor boundaries. In a recent study, the known spectral signatures of glioblastoma were used for boundary delineation[3]. Two-color stimulated Raman spectroscopy has also been used delineate brain tumor boundaries[130]. The delineated boundaries coincided with those manually mapped on H&E-stained slides by a surgical pathologist. It was established using mice models that two-color stimulated Raman spectroscopy could effectively map brain tumor boundaries *in vivo* that appeared generally normal under standard bright-field circumstances. However, none of the studies mentioned above incorporated chemotherapeutic nanomaterials as agents for brain tumor boundary delineation.

In brain tumors, our research group has also leveraged the overexpressed Y_1 receptor protein in an assortment of brain tumor cells such as glioma cells to develop a Y_1 ligand (AP)-conjugated nanomaterial-based delivery system[131]. This afforded a DOX-loaded nano-micelle that circumvents the highly impenetrable blood–brain barrier to specifically target glioma cells (Fig. 7A). The Y_1 ligand (AP)-conjugation effectively stabilizes the nano-micelle in physiological environment and facilitates DOX pH-responsive release in tumor microenvironment. Interestingly, the an IRDye 800CW component also enabled the determination of tumor boundary in mice brain (Fig. 7B), which is highly desirable for ascertaining the actual location, size and boundary of tumor during the tedious surgical resection of brain tumors.

4.2. Breast tumor

Efforts have been made to adequately map breast tumor boundaries using various techniques. Benign breast tumor has been differentiated from the malignant counterpart in an early study by proper tumor boundary mapping technique[132]. The authors proposed an area-based measurement of image edge profile acutance that elucidates the transition in density of an area of interest along

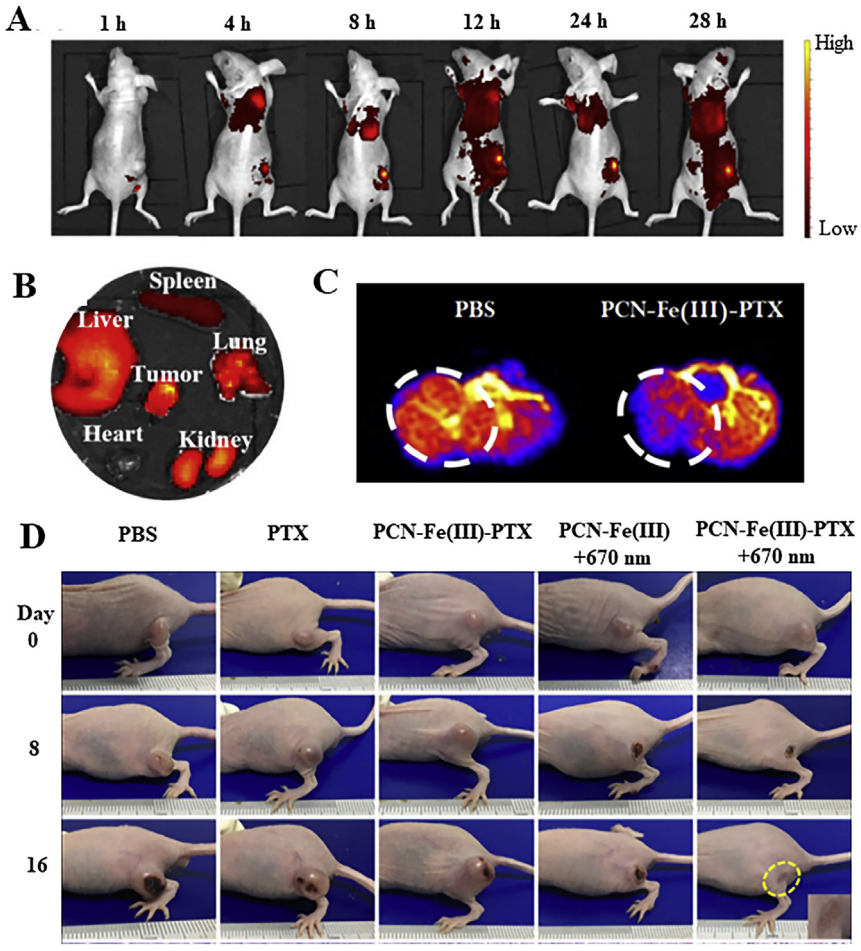

Figure 6 (A) Mice with PANC-1 tumors were imaged fluorescently at the indicated time after intravenous PCN-Fe(III) injection. (B) Fluorescent images of tumors and primary organs 28 h post-injection. (C) *In vivo* T_1-weighted MR imaged from mice administered PCN-Fe(III)-PTX. (D) The real photographs of mice in all five groups on different days after PTX chemotherapeutic drug-enhanced photodynamic therapy. Adapted with permission from Ref. 114. Copyright©2020, Tsinghua University Press and Springer-Verlag GmbH Germany.

normal to the area of interest at all boundary pixels. This also entailed an investigation of the potential of acutance in quantitatively determining the breast tumor boundaries. They observed that acutance alone could differentiate benign and malignant tumor up to 95% of accuracy level, based on their boundaries.

NIR-dye-labeled theranostic nanoparticles in drug resistant breast tumor cells were synthesized to map breast tumor boundaries[30]. Importantly, systemic delivery of the tumor-targeted nanoprobes in mice orthotopic human breast or murine breast tumor model led to extensive accumulation of the nanoprobes in tumor and stromal cells, enabling adequate tumor boundary mapping by fluorescence imaging. At 24 h post-intravenous injection, it was reported that the nanoparticles adequately mapped the tumor boundary in human breast cancer cells MDA-MB-231 (Fig. 8A) but not in murine breast cancer cells 4T1 (Fig. 8B). Fluorescence imaging of DCIS tumor remaining after tumor-targeted therapy using the theranostic nanoparticles was also conducted (Fig. 8C), while Prussian blue staining analysis revealed high amount of the tumor-targeted nanoparticles in the edge of the tumor (Fig. 8D). After four treatments, the residual tumor showed strong fluorescent signal. CD 31 and CD 68 positive tumor blood vessels and macrophages, respectively, were found in the tumor stromal region (purple arrows) but only a hand full occurred within the tumor nodules (yellow arrows). Prussian blue staining revealed a low amount of blue iron positive cells in the necrotic tumor region (yellow arrow) and a high level of blue iron positive cells in the tumor stroma (blue arrow).

Raman spectroscopy and fluorescence imaging have been used in combination to provide a synergistic approach towards breast tumor boundary delineation[112]. The approach holds strong promise in tumor delineation considering the advancements in Raman spectroscopic instrumentation, fibre optical probe modality, and high accuracy delectation device. In mammogram images, the breast region was adequately delineated to provide information on the actual location and tumor volume[63]. Breast tumor boundaries have also been successfully delineated by fluorescence imaging[29]. The strategy involved injecting a targeted contrast agent to enhance the fluorescence signal contrast at the boundaries. Not just that the approach effectively delineated the boundaries of breast tumor, it could also detect residual tumors even at small contrast agent concentrations in such tumors. Another study also successfully used DOX-loaded liposome nanoparticles to delineate murine breast tumor boundaries by a combination of ultrasound and fluorescence imaging[58]. The chemotherapeutic nanomaterial described by the authors also had

Table 1 Advantages and disadvantages of imaging modalities used for tumor boundary delineation.

Imaging modality	Advantage	Disadvantage	Ref.
Fluorescence	Non-invasiveness No ionizing radiation Low acquisition time High sensitivity Inexpensive	Relatively low spatial resolution Limited tissue depth penetration Whole body imaging not possible Potential contrast agent toxicity	116,117
MRI	Non-invasiveness High spatial resolution Unlimited tissue depth penetration Non-ionizing radiation Excellent soft tissue contrast Whole body imaging possible	Relatively low sensitivity Expensive Long acquisition time Potential contrast agent toxicity Not suitable for patients with implants	118−120
Ultrasound	Non-invasiveness Low acquisition time Low cost No ionizing radiation High sensitivity	Whole body imaging not possible Limited spatial resolution Unsuitable for digestive organs Data is difficult to quantify	118,119
Mammography	Inexpensive Low acquisition time	Radiation risk Overdiagnosis False positive and false negative results Data is difficult to quantify	116,121
Raman	Non-invasive Labe-free High specificity Minimal water interference	Sample-dependent autofluorescence Low sensitivity Long acquisition time Expensive Sophisticated data analysis often required	122,123
Endoscopy	No external scar Real-time visualization Could serve as light source for other tumor therapies	Expensive Long acquisition time	124,125
CT	Non-invasiveness High contrast resolution Unlimited tissue depth penetration Low acquisition time Whole body imaging possible	High dose of ionizing radiation Limited soft tissue resolution	116,118−120

gold nanoparticles whose photoconversion capability was leveraged to provide tumor photothermal therapy that complimented DOX-mediated chemotherapy.

4.3. *Liver tumor*

Liver tumor boundaries have been delineated using various techniques such as CT imaging[103,133,134], fluorescence imaging[135], and computational framework[136]. Real-time surgical navigation by CT and fluorescence imaging with intraoperatively administered ICG was used to delineate the boundary between liver tumor and surrounding normal tissues[135]. The study involved 50 liver patients whose liver resection boundaries were determined by photodynamic eye. The researchers observed significant fluorescence contrast between liver tumors and normal liver in 32 patients. Portal vein anatomy was examined after the administration of ICG, which enabled observations of boundaries for half of the liver or particular liver sections in nine patients. Moreover, the approach enabled preoperative detection of eight tiny superficial tumors in the patients.

Yu et al.[137] evaluated the capability of As_2O_3 chemotherapeutic nanoparticles as anti-cancer drug to treat liver tumor and map the boundaries. They used CT imaging to measure tumor longest dimension by response evaluation criteria in the liver tumors. The study also determined hepatic toxicity, rate of tumor necrosis, extent of vascular endothelial growth factor, as well as microvessel density. Whereas the As_2O_3 nanoparticles provided chemotherapy, the liver tumor shape was determined by CT imaging, while both outer tumor boundary and inner regions of necrosis were distinctly delineated in H&E images (Fig. 8E). Another study investigated alginate nanoparticles that were modified with glycyrrhetinic acid and loaded with DOX for liver tumor chemotherapy and boundary delineation[138]. After tail-vein injection in mice, DOX concentration reached 67 μg/g and offered more than 4-fold increase in liver chemotherapy compared to free DOX. Moreover, the liver tumor boundary was adequately mapped in H&E images enabled by DOX-mediated necrosis. Also, glycyrrhetinic acid-modified hyaluronic acid nanoparticles that were loaded with docetaxel showed substantial liver tumor chemotherapy and boundary mapping[139]. The glycyrrhetinic acid-based nanoparticles were modified with hyaluronic acid to obtain the monodispersed nanocarrier of 208 nm size and surface charge of −27 mV for conveying docetaxel to liver tumor site. The high drug loading capacity (12.59) and encapsulation efficiency (85%) of the chemotherapeutic nanomaterial enabled adequate suppression of HepG2 tumor cells growth and boundary mapping my confocal imaging.

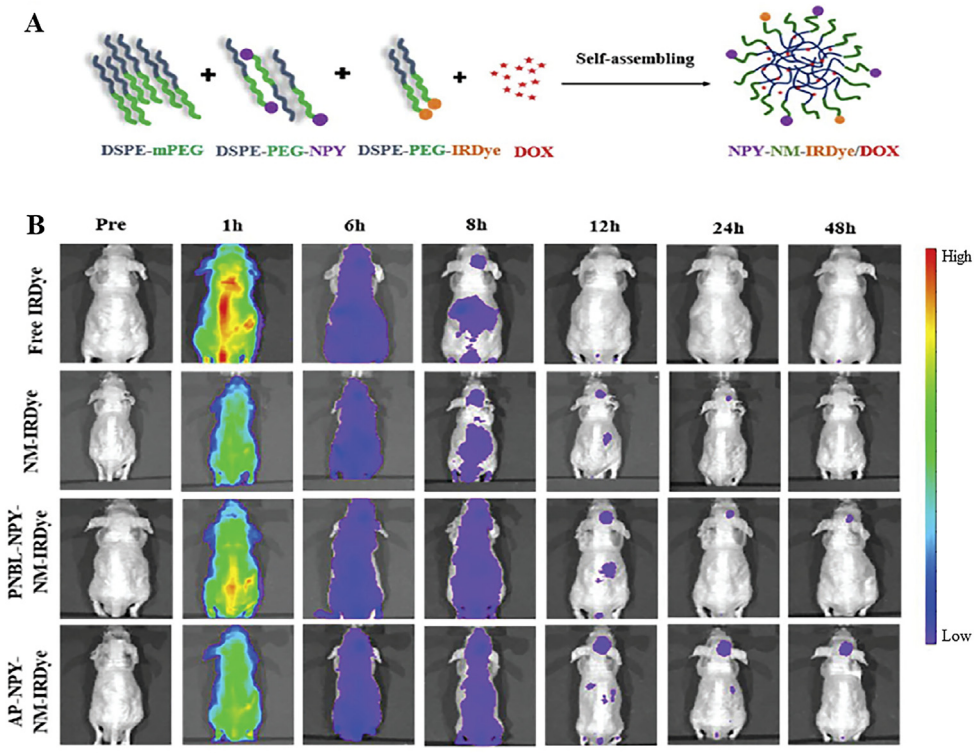

Figure 7 (A) Schematic illustration of the synthesis of neuropeptide Y_1Rs ligand-modified nano-micelles (NPY-NM-IRDye/DOX) through a self-assembling method. (B) *In vivo* fluorescence imaging of U87MG glioma-bearing mice before and after intravenous injection of Y1Rs ligand-modified NM-IRDye through the tail vein. Adapted with permission from Ref. 131. Copyright©2018, Royal Society of Chemistry.

Chemotherapy was combined with photodynamic therapy in another study to treat liver tumor and map their boundaries[140]. The pH-responsive chemotherapeutic nanomaterial featured Pluronic F127−lenvatinib-encapsulated halogenated boron-dipyrromethene nanoparticles for on-demand delivery of the anti-cancer drug lenvatinib, where the boron-dipyrromethene converted near infrared light to produce reactive oxygen species in the liver tumor site to cause synergistic therapy. Moreover, confocal imaging enabled effective delineation of the liver tumor cells. Edabi et al.[141] investigated the efficacy of sorafenib loaded in polyvinyl alcohol and polyethylene glycol matrix with superparamagnetic iron oxide nanoparticles as the core as a chemotherapeutic nanomaterial for liver tumor treatment. They subsequently recorded a 74% sorafenib release at pH 4.8 in a pseudo-second

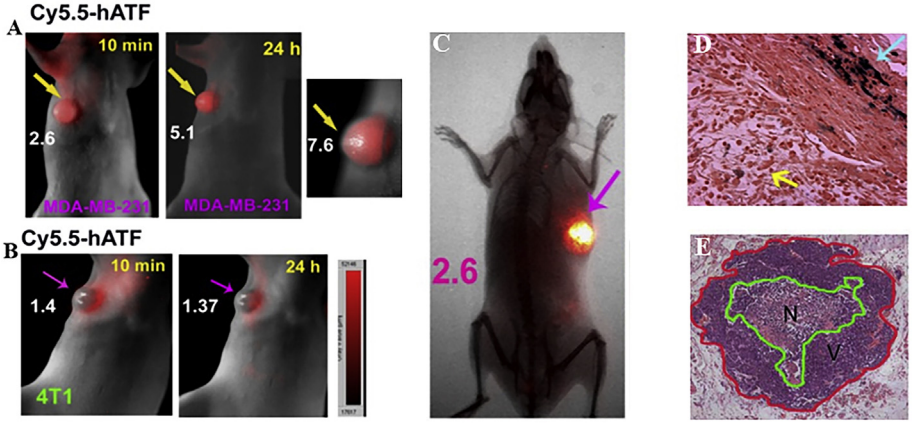

Figure 8 Cy5.5-human peptides injected *via* the tail vein into nude mice bearing either (A) MDA-MB-231 human breast cancer xenografts or (B) 4T1 mouse mammary tumor in the mammary fat pad. (C) NIR optical imaging, immunofluorescence, and (D) Prussian blue staining of the tumors. Adapted with permission from Ref. 29. Copyright©2013, Ivyspring International Publisher. (E) H&E histological image of liver tumor showing both an outer tumor border (red line) and inner regions of necrosis (green line). N and V represent necrosis and viable tumor, respectively. Adapted with permission from Ref. 137. Copyright©2011, Creative Commons Attribution License.

order release kinetics. The robustness of the smart chemotherapeutic nanomaterial could be more meaningfully leveraged for *in vivo* application and subsequent tumor boundary delineation.

4.4. Prostate, gastric and other tumors

Prostate tumor boundaries in mouse model were mapped by NIR and fluorescence imaging following orthotopic implantation[28]. The study used human prostate cancer cells which express a gene reporter that was leveraged to accurately map the tumor cell boundaries with a targeted NIR fluorescent antibody-based probe. The novel gene reporter was effectively targeted by the antibody-based probe, thus enabling adequate probe localization in the prostate tumor cells and subsequent accurate tumor boundary mapping. The study also provided a very useful advancement in bioimaging for guiding intraoperative procedures.

Gastric tumor boundaries have been successfully delineated by endoscopy in various literature reports[97,98,142]. The approach generally involves obtaining images of the tumors in bright field, followed by sprinkling with popular agents such as indigo carmine to expose the tumor boundaries. Conventionally, gastric tumor boundaries could be delineated by endoscopy following ESD, graphic software application or combination of ESD with tiling method. The approach is usually complemented with histopathological analysis to further provide information on the boundaries and tumor lesions. Chemotherapeutic nanomaterials have been successfully deployed to map the boundaries of prostate tumors. As a paradigm, SERS imaging was deployed in an anti-cancer docetaxel-loaded chemotherapeutic nanomaterial to detect prostrate tumors[87]. Importantly also, the docetaxel moiety provided effective tumor chemotherapy. The study could be leveraged to predict docetaxel response in cancer patients which could provide information on effective image-guided chemotherapy of prostate tumors. A multifunctional endoscope system was utilized to effectively map the boundaries of gastric tumors using DOX-loaded chemotherapeutic nanomaterial[101]. Interestingly, the nanomaterial design strategy featured incorporation of gold nanoparticles for gastric tumor killing by photothermal therapy, a photosensitizer chlorin e6 to offer photodynamic therapy and the thermosensitive poly(*N*-isopropylacrylamide) shell that protected the anticancer drug DOX from release prior to endoscopic laser irradiation.

A chemotherapeutic nanomaterial was also used to map the boundary of ovarian cancer by SERS imaging[91]. The nanomaterial comprised of an anti-cancer drug DOX which was responsible for the pH-triggered tumor chemotherapy. Moreover, the light-to-heat conversion capability of gold nanoparticles in the chemotherapeutic nanomaterial was leveraged to provide photothermal therapy, resulting in substantial ovarian tumor regression within 15 days of the synergistic treatment. Another study also used SERS imaging to map the boundary of bladder tumor[143]. The researchers used both passive (antibody-based) and active (tissue permeability-based) targeting mechanisms for evaluation *via ex vivo* topical application of nanoparticles to sessions of human bladder tissue. They observed 5-fold deeper penetration and binding to bladder tumor tissue during passive targeting in comparison with normal bladder urothelium. This suggested the existence of an enhanced permeability and retention effect in human bladder tumor that enabled boundary delineation. Bladder tumor boundary delineation was clear in the biomarker CA9 staining histological image but quite vague in the H&E and Raman images.

5. Conclusions and future perspectives

Accurately delineating tumor boundaries is very crucial in tumor therapy, to enable targeting residual malignant tissues near the tumor boundaries. Presently, by applying various advanced imaging modalities either singly or in combination (multimodal imaging), tumor identification and accurate boundary delineation could be achieved in various tumor types. Various strategies including fluorescence imaging, MRI, ultrasound imaging, CT, Raman imaging, endoscopy, mammography, and multimodal imaging have been used to delineate the boundaries of brain, breast, liver, prostate, gastric, ovarian and bladder tumors using chemotherapeutic nanomaterials as agents, and their successes and challenges in tumor boundary delineation were extensively discussed in this review. Advances made in our research group about using nanomaterial-based drug delivery systems loaded with various bioimaging agents as potential tumor boundary delineating agents were also showcased in detail.

Notwithstanding that multimodal imaging has shown significant promise in delineating tumor boundaries, we believe that its application in brain tumor boundary delineation has yet to be adequately achieved which will entail more in-depth research and optimization. The various researches involving nanomaterial-based drug delivery systems using single-modal imaging modality to delineate tumor margins also need to be matched with various other techniques, especially model and algorithms, to achieve more meaningful tumor boundary delineation. Also, such efforts can possibly herald the incorporation of models and algorithms in 3D boundary detection of brain tumors. We therefore believe that more research can be channeled toward proffering solutions to those critical issues.

Moreover, we believe that such efforts can possibly herald the incorporation of models and algorithms in 3D boundary detection of brain tumors. In as much as intraoperative MRI can help to map glioma boundary by multiple scanning sequences, it is obvious that such increases in scanning sequences will elongate the operative time, necessitate using anesthesia, and increase the chances of patients developing infections. We believe that further research is required for some imaging modalities such as MRI, Raman and endoscopy by optimizing the scanning sequence, shortening the time of scanning, and enhancing image accuracy and corresponding quality. In general, we believe that with continuous advancements in understanding, research, and technology, the nanomaterials-based chemotherapeutic treatment of tumors will eventually attain a state of “total and safe tumor regression”, and with relentless research efforts, it will be possible to develop nanomaterial-based drug delivery systems with formidable capability for tumor boundary delineation.

Acknowledgments

This work was supported by the funding from National Natural Science Foundation of China (32025021 and 31971292), Strategic Priority Research Program of Chinese Academy of Sciences, Grant/Award Number: XDB36000000, and National Key R&D Program of China (2019YFA0405603).

Author contributions

Ozioma Udochukwu Akakuru and Zhoujing Zhang wrote the manuscript. M. Zubair Iqbal, Chengjie Zhu, and Yewei Zhang reviewed and edited the manuscript. Aiguo Wu conceptualized the project, harmonized the structure, and is the corresponding author.

Conflicts of interest

The authors have no conflicts of interest to declare.

References

1. Hamstra D, Galbán C, Meyer C, Johnson T, Sundgren P, Tsien C, et al. Functional diffusion map as an early imaging biomarker for high-grade glioma: correlation with conventional radiologic response and overall survival. *J Clin Oncol* 2008;**26**:3387−94.
2. Moffat BA, Chenevert TL, Meyer CR, McKeever PE, Hall DE, Hoff BA, et al. The functional diffusion map: an imaging biomarker for the early prediction of cancer treatment outcome. *Neoplasia* 2006;**8**:259−67.
3. Ross W, Tucker M, Ma G, Codd P. Model for and analysis of intraoperative brain tumor boundary detection based on known spectral signatures of glioblastoma. In: *Proceedings volume 11229, advanced biomedical and clinical diagnostic and surgical guidance systems XVIII; 1122918 (2020)*. San Francisco, CA, USA: SPIE BiOS; 2020. Available from: https://doi.org/10.1117/12.2546329.
4. Zhao BW, Poo MM. An interview with Mingjie Zhang: phase separation in biological systems. *Natl Sci Rev* 2021;**8**:nwab081.
5. Brangwynne CP, Eckmann CR, Courson DS, Rybarska A, Hoege C, Gharakhani J, et al. Germline P granules are liquid droplets that localize by controlled dissolution/condensation. *Science* 2009;**324**:1729−32.
6. Young RM, Jamshidi A, Davis G, Sherman JH. Current trends in the surgical management and treatment of adult glioblastoma. *Ann Transl Med* 2015;**3**:121.
7. Lim EK, Kim T, Paik S, Haam S, Huh YM, Lee K. Nanomaterials for theranostics: recent advances and future challenges. *Chem Rev* 2015;**115**:327−94.
8. Hadjipanayis CG, Widhalm G, Stummer W. What is the surgical benefit of utilizing 5-aminolevulinic acid for fluorescence-guided surgery of malignant gliomas?. *Neurosurgery* 2015;**77**:663−73.
9. Akakuru OU, Iqbal MZ, Saeed M, Liu C, Paunesku T, Woloschak G, et al. The transition from metal-based to metal-free contrast agents for T1 magnetic resonance imaging enhancement. *Bioconjugate Chem* 2019;**30**:2264−86.
10. Enwereuzo OO, Akakuru OC, Uwaoma RC, Elemike EE, Akakuru OU. Self-assembled membrane-polymer nanoparticles of top-notch tissue tolerance for the treatment of gastroesophageal reflux disease. *J Nanostructure Chem* 2021;**11**:707−19.
11. Akakuru OU, Louis H, Uwaoma R, Elemike EE, Akakuru OC. Novel highly-swellable and pH-responsive slow release formulations of clotrimazole with chitosan-*g*-PEG/starch microparticles. *React Funct Polym* 2019;**135**:32−43.
12. Akakuru OU, Louis H, Akakuru OC, Eno EA. Facile fabrication of pH-responsive and swellable slow release microparticles of chlorpheniramine maleate with chitosan-starch matrices and their cross-links. *Int J Polym* 2020;**69**:269−83.
13. Fu S, Li G, Zang W, Zhou X, Shi K, Zhai Y. Pure drug nano-assemblies: a facile carrier-free nanoplatform for efficient cancer therapy. *Acta Pharm Sin B* 2021;**11**:3636−47.
14. Jiang Z, Wang Y, Sun L, Yuan B, Tian Y, Xiang L, et al. Dual ATP and pH responsive ZIF-90 nanosystem with favorable biocompatibility and facile post-modification improves therapeutic outcomes of triple negative breast cancer *in vivo*. *Biomaterials* 2019;**197**:41−50.
15. Xing Y, Jiang Z, Akakuru OU, He Y, Li A, Li J, et al. Mitochondria-targeting zeolitic imidazole frameworks to overcome platinum-resistant ovarian cancer. *Colloids Surf B Biointerfaces* 2020;**189**:110837.
16. Jiang Z, Li Y, Wei Z, Yuan B, Wang Y, Akakuru OU, et al. Pressure-induced amorphous zeolitic imidazole frameworks with reduced toxicity and increased tumor accumulation improves therapeutic efficacy *in vivo*. *Bioact Mater* 2021;**6**:740−8.
17. Balch GC, Mithani SK, Simpson JF, Kelley MC. Accuracy of intraoperative gross examination of surgical margin status in women undergoing partial mastectomy for breast malignancy. *Ann Surg* 2005;**71**:22−7.
18. Lee J, Lee S, Bae Y. Multiple margin positivity of frozen section is an independent risk factor for local recurrence in breast-conserving surgery. *J Breast Cancer* 2012;**15**:420−6.
19. Konstantinidis IT, Warshaw AL, Allen JN, Blaszkowsky LS, Castillo CF, Deshpande V, et al. Pancreatic ductal adenocarcinoma: is there a survival difference for R1 resections versus locally advanced unresectable tumors? What is a "true" R0 resection? *Ann Surg* 2013;**257**:731−6.
20. Assersohn L, Powles TJ, Ashley S, Nash AG, Neal AJ, Sacks N, et al. Local relapse in primary breast cancer patients with unexcised positive surgical margins after lumpectomy, radiotherapy and chemo-endocrine therapy. *Ann Oncol* 1999;**10**:1451−5.
21. Abraham SC, Fox K, Fraker D, Solin L, Reynolds C. Sampling of grossly benign breast reexcisions: a multidisciplinary approach to assessing adequacy. *Am J Surg Pathol* 1999;**23**:316−22.
22. Sahoo S, Lester SC. Pathology of breast carcinomas after neoadjuvant chemotherapy: an overview with recommendations on specimen processing and reporting. *Arch Pathol Lab Med* 2009;**133**:633−42.
23. Jung W, Kang E, Kim SM, Kim D, Hwang Y, Sun Y, et al. Factors associated with re-excision after breast-conserving surgery for early-stage breast cancer. *J Breast Cancer* 2012;**15**:412−9.
24. van Dam GM, Themelis G, Crane LMA, Harlaar NJ, Pleijhuis RG, Kelder W, et al. Intraoperative tumor-specific fluorescence imaging in ovarian cancer by folate receptor-α targeting: first in-human results. *Nat Med* 2011;**17**:1315−9.
25. Ye Y, Bloch S, Xu B, Achilefu S. Design, synthesis, and evaluation of near infrared fluorescent multimeric RGD peptides for targeting tumors. *J Med Chem* 2006;**49**:2268−75.
26. Ke S, Wen X, Gurfinkel M, Charnsangavej C, Wallace S, Sevick-Muraca EM, et al. Near-infrared optical imaging of epidermal growth factor receptor in breast cancer xenografts. *Cancer Res* 2003;**63**:7870−5.
27. Akakuru OU, Liu C, Iqbal MZ, Dar GI, Yang G, Qian K, et al. A hybrid organo-nanotheranostic platform of superlative biocompatibility for near-infrared-triggered fluorescence imaging and synergistically enhanced ablation of tumors. *Small* 2020;**16**:2002445.
28. Zhu B, Wu G, Robinson H, Wilganowski N, Hall MA, Ghosh SC, et al. Tumor margin detection using quantitative NIRF molecular imaging targeting EpCAM validated by far red gene reporter iRFP. *Mol Imag Biol* 2013;**15**:560−8.
29. Yang L, Sajja HK, Cao Z, Qian W, Bender L, Marcus AI, et al. uPAR-targeted optical imaging contrasts as theranostic agents for tumor margin detection. *Theranostics* 2013;**4**:106−18.
30. Blasi F, Carmeliet P. uPAR: a versatile signalling orchestrator. *Nat Rev Mol Cell Biol* 2002;**3**:932−43.
31. Wu X, Yin C, Ma J, Chai S, Zhang C, Yao S, et al. Polyoxypregnanes as safe, potent, and specific ABCB1-inhibitory pro-drugs to overcome multidrug resistance in cancer chemotherapy *in vitro* and *in vivo*. *Acta Pharm Sin B* 2021;**11**:1885−902.
32. Wang Y, Jiang Z, Yuan B, Tian Y, Xiang L, Li Y, et al. A Y1 receptor ligand synergized with a P-glycoprotein inhibitor improves the therapeutic efficacy of multidrug resistant breast cancer. *Biomater Sci* 2019;**7**:4748−57.
33. Zhang R, Xing R, Jiao T, Ma K, Chen C, Ma G, et al. Carrier-free, chemophotodynamic dual nanodrugs *via* self-assembly for synergistic antitumor therapy. *ACS Appl Mater Interfaces* 2016;**8**:13262−9.
34. Tian F, Conde J, Bao C, Chen Y, Curtin J, Cui D. Gold nanostars for efficient *in vitro* and *in vivo* real-time SERS detection and drug delivery *via* plasmonic-tunable Raman/FTIR imaging. *Biomaterials* 2016;**106**:87−97.
35. Akakuru OU, Xu C, Liu C, Li Z, Xing J, Pan C, et al. Metal-free organo-theranostic nanosystem with high nitroxide stability and loading for image-guided targeted tumor therapy. *ACS Nano* 2021;**15**:3079−97.
36. Akakuru OU, Iqbal MZ, Liu C, Xing J, Wei Z, Jiang Z, et al. Self-assembled, biocompatible and biodegradable TEMPO-conjugated

nanoparticles enable folate-targeted tumor magnetic resonance imaging. *Appl Mater Today* 2020;**18**:100524.
37. Law AKW, Zhu H, Lam FK, Chan HY, Chan BCB, Iu PP. Tumor boundary extraction in multislice MR brain images using region and contour deformation. *Proc MIAR* 2001:183−7.
38. Kubben PL, ter Meulen KJ, Schijns OE, ter Laak-Poort MP, van Overbeeke JJ, van Santbrink H. Intraoperative MRI-guided resection of glioblastoma multiforme: a systematic review. *Lancet Oncol* 2011;**12**:1062−70.
39. Lin Y, Yang X. Surgical resection of glioma involving eloquent brain areas: tumor boundary, functional boundary, and plasticity consideration. *Glioma* 2020;**3**:53−60.
40. Jiang Z, Yuan B, Qiu N, Wang Y, Sun L, Wei Z, et al. Manganese-zeolitic imidazolate frameworks-90 with high blood circulation stability for MRI-guided tumor therapy. *Nano-Micro Lett* 2019;**11**:61.
41. Jiang Z, Tian Y, Shan D, Wang Y, Gerhard E, Xia J, et al. pH protective Y1 receptor ligand functionalized antiphagocytosis BPLP-WPU micelles for enhanced tumor imaging and therapy with prolonged survival time. *Biomaterials* 2018;**170**:70−81.
42. Cao Y, Jiang Z, Li Y, Wang Y, Yang Y, Akakuru OU, et al. Tandem post-synthetic modification of a zeolitic imidazolate framework for CXCR4-overexpressed esophageal squamous cell cancer imaging and therapy. *Nanoscale* 2020;**12**:12779−89.
43. Wu C, Han D, Chen T, Pen L, Zhu G, You M, et al. Building a multifunctional aptamer-based DNA nanoassembly for targeted cancer therapy. *J Am Chem Soc* 2013;**135**:18644−50.
44. Ponce AM, Viglianti BL, Yu D, Yarmolenko PS, Michelich CR, Woo J, et al. Magnetic resonance imaging of temperature-sensitive liposome release: drug dose painting and antitumor effects. *J Natl Cancer Inst* 2007;**99**:53−63.
45. Tao K, Liu S, Wang L, Qiu H, Li B, Zhang M, et al. Targeted multifunctional nanomaterials with MRI, chemotherapy and photothermal therapy for the diagnosis and treatment of bladder cancer. *Biomater Sci* 2020;**8**:342−52.
46. Wang D, Lin H, Zhang G, Si Y, Yang H, Bai G, et al. Effective pH-activated theranostic platform for synchronous magnetic resonance imaging diagnosis and chemotherapy. *ACS Appl Mater Interfaces* 2018;**10**:31114−23.
47. Rygh OM, Selbekk T, Torp SH, Lydersen S, Hernes TA, Unsgaard G. Comparison of navigated 3D ultrasound findings with histopathology in subsequent phases of glioblastoma resection. *Acta Neurochir* 2008;**150**:1033−41.
48. Solheim O, Selbekk T, Jakola AS, Unsgård G. Ultrasound-guided operations in unselected high-grade gliomas−overall results, impact of image quality and patient selection. *Acta Neurochir* 2010;**152**:1873−86.
49. Selbekk T, Jakola AS, Solheim O, Johansen TF, Lindseth F, Reinertsen I, et al. Ultrasound imaging in neurosurgery: approaches to minimize surgically induced image artefacts for improved resection control. *Acta Neurochir* 2013;**155**:973−80.
50. Coburger J, Scheuerle A, Thal DR, Engelke J, Hlavac M, Wirtz CR, et al. Linear array ultrasound in low-grade glioma surgery: histology-based assessment of accuracy in comparison to conventional intraoperative ultrasound and intraoperative MRI. *Acta Neurochir* 2015;**157**:195−206.
51. Moiyadi AV, Shetty PM, Mahajan A, Udare A, Sridhar E. Usefulness of three-dimensional navigable intraoperative ultrasound in resection of brain tumors with a special emphasis on malignant gliomas. *Acta Neurochir* 2013;**155**:2217−25.
52. Unsgaard G, Selbekk T, Brostrup Müller T, Ommedal S, Torp SH, Myhr G, et al. Ability of navigated 3D ultrasound to delineate gliomas and metastases−comparison of image interpretations with histopathology. *Acta Neurochir* 2005;**147**:1259−69.
53. Morin F, Courtecuisse H, Reinertsen I, Le Lann F, Palombi O, Payan Y, et al. Brain-shift compensation using intraoperative ultrasound and constraint-based biomechanical simulation. *Med Image Anal* 2017;**40**:133−53.
54. Bucholz RD, Yeh DD, Trobaugh J, McDurmont LL, Sturm CD, Baumann C, et al. *The correction of stereotactic inaccuracy caused by brain shift using an intraoperative ultrasound device*. Berlin: Springer Berlin Heidelberg; 1997. p. 459−66.
55. Piotrzkowska-Wróblewska H, Dobruch-Sobczak K, Klimonda Z, Karwat P, Roszkowska-Purska K, Gumowska M, et al. Monitoring breast cancer response to neoadjuvant chemotherapy with ultrasound signal statistics and integrated backscatter. *PLoS One* 2019;**14**:e0213749.
56. Taleghamar H, Moghadas-Dastjerdi H, Czarnota GJ, Sadeghi-Naini A. Characterizing intra-tumor regions on quantitative ultrasound parametric images to predict breast cancer response to chemotherapy at pre-treatment. *Sci Rep* 2021;**11**:14865.
57. Rapoport N, Gao Z, Kennedy A. Multifunctional nanoparticles for combining ultrasonic tumor imaging and targeted chemotherapy. *J Natl Cancer Inst* 2007;**99**:1095−106.
58. Li W, Hou W, Guo X, Luo L, Li Q, Zhu C, et al. Temperature-controlled, phase-transition ultrasound imaging-guided photothermal-chemotherapy triggered by NIR light. *Theranostics* 2018;**8**:3059−73.
59. Mustra M, Grgic M, Rangayyan RM. Review of recent advances in segmentation of the breast boundary and the pectoral muscle in mammograms. *Med Biol Eng Comput* 2016;**54**:1003−24.
60. Sterns EE. Relation between clinical and mammographic diagnosis of breast problems and the cancer/biopsy rate. *Can J Surg* 1996;**39**:128−32.
61. Highnam R, Brady M. A model of mammogram image formation. In: *Mammographic image analysis. Netherlands*. Dordrecht: Springer Netherlands; 1999. p. 31−55.
62. Mustra M, Grgic M. Robust automatic breast and pectoral muscle segmentation from scanned mammograms. *Signal Process* 2013;**93**:2817−27.
63. Zebari DA, Zeebaree DQ, Abdulazeez A, Haron H, Hamed HNA. Improved threshold based and trainable fully automated segmentation for breast cancer boundary and pectoral muscle in mammogram images. *IEEE Access* 2020;**8**:203097−116.
64. Torrisi L, Restuccia N, Torrisi A. Study of gold nanoparticles for mammography diagnostic and radiotherapy improvements. *Rep Practical Oncol Radiother* 2019;**24**:450−7.
65. Hsu JC, Cruz ED, Lau KC, Bouché M, Kim J, Maidment ADA, et al. Renally excretable and size-tunable silver sulfide nanoparticles for dual-energy mammography or computed tomography. *Chem Mater* 2019;**31**:7845−54.
66. Lu C, Chen G, Yu B, Cong H. Recent advances of low biological toxicity Ag_2S QDs for biomedical application. *Adv Eng Mater* 2018;**20**:1700940.
67. Hsu JC, Naha PC, Lau KC, Chhour P, Hastings R, Moon BF, et al. An all-in-one nanoparticle (AION) contrast agent for breast cancer screening with DEM-CT-MRI-NIRF imaging. *Nanoscale* 2018;**10**:17236−48.
68. Kalkanis SN, Kast RE, Rosenblum ML, Mikkelsen T, Yurgelevic SM, Nelson KM, et al. Raman spectroscopy to distinguish grey matter, necrosis, and glioblastoma multiforme in frozen tissue sections. *J Neuro Oncol* 2014;**116**:477−85.
69. Jermyn M, Desroches J, Mercier J, St-Arnaud K, Guiot MC, Leblond F, et al. Raman spectroscopy detects distant invasive brain cancer cells centimeters beyond MRI capability in humans. *Biomed Opt Express* 2016;**7**:5129−37.
70. Lin J, Yu J, Akakuru OU, Wang X, Yuan B, Chen T, et al. Low temperature-boosted high efficiency photo-induced charge transfer for remarkable SERS activity of ZnO nanosheets. *Chem Sci* 2020;**11**:9414−20.
71. Lin J, Hao W, Shang Y, Wang X, Qiu D, Ma G, et al. Direct Experimental observation of facet-dependent SERS of Cu_2O polyhedra. *Small* 2018;**14**:1703274.
72. Nicolson F, Jamieson LE, Mabbott S, Plakas K, Shand NC, Detty MR, et al. Surface enhanced resonance Raman spectroscopy

(SERRS) for probing through plastic and tissue barriers using a handheld spectrometer. *Analyst* 2018;**143**:5965−73.
73. Grytsyk N, Boubegtiten-Fezoua Z, Javahiraly N, Omeis F, Devaux E, Hellwig P. Surface-enhanced resonance Raman spectroscopy of heme proteins on a gold grid electrode. *Spectrochim Acta* 2020;**230**: 118081.
74. Freudiger CW, Min W, Saar BG, Lu S, Holtom GR, He C, et al. Label-free biomedical imaging with high sensitivity by stimulated Raman scattering microscopy. *Science* 2008;**322**:1857−61.
75. Ploetz E, Laimgruber S, Berner S, Zinth W, Gilch P. Femtosecond stimulated Raman microscopy. *Appl Phys B* 2007;**87**:389−93.
76. Zumbusch A, Holtom GR, Xie XS. Three-dimensional vibrational imaging by coherent anti-Stokes Raman scattering. *Phys Rev Lett* 1999;**82**:4142−5.
77. Evans CL, Xie XS. Coherent anti-Stokes Raman scattering microscopy: chemical imaging for biology and medicine. *Annu Rev Anal Chem* 2008;**1**:883−909.
78. Auner GW, Koya SK, Huang C, Broadbent B, Trexler M, Auner Z, et al. Applications of Raman spectroscopy in cancer diagnosis. *Cancer Metastasis Rev* 2018;**37**:691−717.
79. Pohling C, Buckup T, Pagenstecher A, Motzkus M. Chemoselective imaging of mouse brain tissue *via* multiplex CARS microscopy. *Biomed Opt Express* 2011;**2**:2110−6.
80. Freudiger CW, Pfannl R, Orringer DA, Saar BG, Ji M, Zeng Q, et al. Multicolored stain-free histopathology with coherent Raman imaging. *Lab Invest* 2012;**92**:1492−502.
81. Evans CL, Potma EO, Puoris'haag M, Côté D, Lin CP, Xie XS. Chemical imaging of tissue *in vivo* with video-rate coherent anti-Stokes Raman scattering microscopy. *Proc Natl Acad Sci U S A* 2005;**102**:16807−12.
82. Saar BG, Freudiger CW, Reichman J, Stanley CM, Holtom GR, Xie XS. Video-rate molecular imaging *in vivo* with stimulated Raman scattering. *Science* 2010;**330**:1368.
83. Horton NG, Wang K, Kobat D, Clark CG, Wise FW, Schaffer CB, et al. In vivo three-photon microscopy of subcortical structures within an intact mouse brain. *Nat Photonics* 2013;**7**:205−9.
84. Fu D, Lu FK, Zhang X, Freudiger C, Pernik DR, Holtom G, et al. Quantitative chemical imaging with multiplex stimulated Raman scattering microscopy. *J Am Chem Soc* 2012;**134**:3623−6.
85. Li Y, Wei Q, Ma F, Li X, Liu F, Zhou M. Surface-enhanced Raman nanoparticles for tumor theranostics applications. *Acta Pharm Sin B* 2018;**8**:349−59.
86. Harmsen S, Bedics MA, Wall MA, Huang R, Detty MR, Kircher MF. Rational design of a chalcogenopyrylium-based surface-enhanced resonance Raman scattering nanoprobe with attomolar sensitivity. *Nat Commun* 2015;**6**:6570.
87. Hu J, Shao X, Chi C, Zhu Y, Xin Z, Sha J, et al. Surface-enhanced Raman spectroscopy of serum predicts sensitivity to docetaxel-based chemotherapy in patients with metastatic castration-resistant prostate cancer. *J Innov Opt Health Sci* 2021;**14**:2141006.
88. Srinivasan S, Bhardwaj V, Nagasetti A, Fernandez-Fernandez A, McGoron AJ. Multifunctional surface-enhanced Raman spectroscopy-detectable silver nanoparticles combined photodynamic therapy and pH-triggered chemotherapy. *J Biomed Nanotechnol* 2016;**12**:2202−19.
89. He J, Dong J, Hu Y, Li G, Hu Y. Design of Raman tag-bridged core−shell Au@$Cu_3(BTC)_2$ nanoparticles for Raman imaging and synergistic chemo-photothermal therapy. *Nanoscale* 2019;**11**: 6089−100.
90. Pal S, Ray A, Andreou C, Zhou Y, Rakshit T, Wlodarczyk M, et al. DNA-enabled rational design of fluorescence-Raman bimodal nanoprobes for cancer imaging and therapy. *Nat Commun* 2019;**10**: 1926.
91. Zhang Y, Liu Z, Thackray BD, Bao Z, Yin X, Shi F, et al. Intraoperative Raman-guided chemo-photothermal synergistic therapy of advanced disseminated ovarian cancers. *Small* 2018;**14**:1801022.
92. Mouri R, Yoshida S, Tanaka S, Oka S, Yoshihara M, Chayama K. Evaluation and validation of computed virtual chromoendoscopy in early gastric cancer. *Gastrointest Endosc* 2009;**69**:1052−8.
93. Pohl J, May A, Rabenstein T, Pech O, Ell C. Computed virtual chromoendoscopy: a new tool for enhancing tissue surface structures. *Endoscopy* 2007;**39**:80−3.
94. Osawa H, Yoshizawa M, Yamamoto H, Kita H, Satoh K, Ohnishi H, et al. Optimal band imaging system can facilitate detection of changes in depressed-type early gastric cancer. *Gastrointest Endosc* 2008;**67**:226−34.
95. Kaise M, Kato M, Urashima M, Arai Y, Kaneyama H, Kanzazawa Y, et al. Magnifying endoscopy combined with narrow-band imaging for differential diagnosis of superficial depressed gastric lesions. *Endoscopy* 2009;**41**:310−5.
96. Nakayoshi T, Tajiri H, Matsuda K, Kaise M, Ikegami M, Sasaki H. Magnifying endoscopy combined with narrow band imaging system for early gastric cancer: correlation of vascular pattern with histopathology (including video). *Endoscopy* 2004;**36**:1080−4.
97. Iizuka T, Kikuchi D, Hoteya S, Yahagi N. The acetic acid + indigocarmine method in the delineation of gastric cancer. *J Gastroenterol Hepatol* 2008;**23**:1358−61.
98. Kawahara Y, Takenaka R, Okada H, Kawano S, Inoue M, Tsuzuki T, et al. Novel chromoendoscopic method using an acetic acid-indigocarmine mixture for diagnostic accuracy in delineating the margin of early gastric cancers. *Dig Endosc* 2009;**21**:14−9.
99. Toyoda H, Rubio C, Befrits R, Hamamoto N, Adachi Y, Jaramillo E. Detection of intestinal metaplasia in distal esophagus and esophagogastric junction by enhanced-magnification endoscopy. *Gastrointest Endosc* 2004;**59**:15−21.
100. Yagi K, Aruga Y, Nakamura A, Sekine A, Umezu H. The study of dynamic chemical magnifying endoscopy in gastric neoplasia. *Gastrointest Endosc* 2005;**62**:963−9.
101. Lee H, Lee Y, Song C, Cho HR, Ghaffari R, Choi TK, et al. An endoscope with integrated transparent bioelectronics and theranostic nanoparticles for colon cancer treatment. *Nat Commun* 2015;**6**:10059.
102. Garai E, Sensarn S, Zavaleta CL, Loewke NO, Rogalla S, Mandella MJ, et al. A Real-time clinical endoscopic system for intraluminal, multiplexed imaging of surface-enhanced Raman scattering nanoparticles. *PLoS One* 2015;**10**:e0123185.
103. Williams DM, Bland P, Liu L, Farjo L, Francis IR, Meyer CR. Liver-tumor boundary detection: human observer *vs* computer edge detection. *Invest Radiol* 1989;**24**:768−75.
104. Xing Y, Zhu J, Zhao L, Xiong Z, Li Y, Wu S, et al. SPECT/CT imaging of chemotherapy-induced tumor apoptosis using ^{99m}Tc-labeled dendrimer-entrapped gold nanoparticles. *Drug Deliv* 2018; **25**:1384−93.
105. Keshavarz M, Moloudi K, Paydar R, Abed Z, Beik J, Ghaznavi H, et al. Alginate hydrogel co-loaded with cisplatin and gold nanoparticles for computed tomography image-guided chemotherapy. *J Biomater Appl* 2018;**33**:161−9.
106. Zheng YTY, Bao Z, Wang H, Ren F, Guo M, Quan H, et al. FePt nanoparticles as a potential X-ray activated chemotherapy agent for HeLa cells. *Int J Nanomed* 2015;**10**:6435−44.
107. Zhu J, Wang G, Alves CS, Tomás H, Xiong Z, Shen M, et al. Multifunctional dendrimer-entrapped gold nanoparticles conjugated with doxorubicin for pH-responsive drug delivery and targeted computed tomography imaging. *Langmuir* 2018;**34**:12428−35.
108. Gempt J, Soehngen E, Förster S, Ryang YM, Schlegel J, Zimmer C, et al. Multimodal imaging in cerebral gliomas and its neuropathological correlation. *Eur J Radiol* 2014;**83**:829−34.
109. Sakurada K, Matsuda K, Funiu H, Kuge A, Takemura S, Sato S, et al. Usefulness of multimodal examination and intraoperative magnetic resonance imaging system in glioma surgery. *Neurol Med -Chir* 2012;**52**:553−7.
110. Tanaka Y, Nariai T, Momose T, Aoyagi M, Maehara T, Tomori T, et al. Glioma surgery using a multimodal navigation system with integrated metabolic images. *J Neurosurg* 2009;**110**:163−72.
111. Nimsky C, Ganslandt O, Hastreiter P, Fahlbusch R. Intraoperative compensation for brain shift. *Surg Neurol* 2001;**56**:357−64.
112. Zhou Y, Liu CH, Li J, Li Z, Zhou L, Chen K, et al. Tumor margin detection using optical biopsy techniques. In: *Proceedings volume*

8940, optical biopsy XII; 894014 (2014). San Francisco, CA, USA: SPIE BiOS; 2014. Available from: https://doi.org/10.1117/12.2038723.
113. Aisen AM, Martel W, Braunstein EM, McMillin KI, Phillips WA, Kling TF. MRI and CT evaluation of primary bone and soft-tissue tumors. *AJR Am J Roentgenol* 1986;**146**:749−56.
114. Zhang T, Jiang Z, Chen L, Pan C, Sun S, Liu C, et al. PCN-Fe(III)-PTX nanoparticles for MRI guided high efficiency chemo-photodynamic therapy in pancreatic cancer through alleviating tumor hypoxia. *Nano Res* 2020;**13**:273−81.
115. Zhang T, Jiang Z, Xve T, Sun S, Li J, Ren W, et al. One-pot synthesis of hollow PDA@DOX nanoparticles for ultrasound imaging and chemo-thermal therapy in breast cancer. *Nanoscale* 2019;**11**:21759−66.
116. Frangioni JV, Hajjar RJ. *In vivo* tracking of stem cells for clinical trials in cardiovascular disease. *Circulation* 2004;**110**:3378−83.
117. Progatzky F, Dallman MJ, Lo Celso C. From seeing to believing: labelling strategies for *in vivo* cell-tracking experiments. *Interface Focus* 2013;**3**:20130001.
118. Cores J, Caranasos TG, Cheng K. Magnetically targeted stem cell delivery for regenerative medicine. *J Funct Biomater* 2015;**6**:526−46.
119. Li X, Zhang XN, Li XD, Chang J. Multimodality imaging in nanomedicine and nanotheranostics. *Cancer Biol Med* 2016;**13**:339−48.
120. Sivasubramanian M, Hsia Y, Lo LW. Nanoparticle-facilitated functional and molecular imaging for the early detection of cancer. *Front Mol Biosci* 2014;**1**:15.
121. Heywang-Köbrunner SH, Hacker A, Sedlacek S. Advantages and disadvantages of mammography screening. *Breast Care* 2011;**6**:199−207.
122. Eberhardt K, Stiebing C, Matthäus C, Schmitt M, Popp J. Advantages and limitations of Raman spectroscopy for molecular diagnostics: an update. *Expert Rev Mol Diagn* 2015;**15**:773−87.
123. Beattie JR, McGarvey JJ, Stitt AW. Raman spectroscopy for the detection of AGEs/ALEs. *Methods Mol Biol* 2013;**965**:297−312.
124. Su PY. Comparison of endoscopic and external dacryocystorhinostomy for treatment of primary acquired nasolacrimal duct obstruction. *Taiwan J Ophthalmol* 2018;**8**:19−23.
125. Amadi AJ. Endoscopic DCR *vs* external DCR: what's best in the acute setting? *J Ophthalmic Vis Res* 2017;**12**:251−3.
126. Cui J, Xu Y, Tu H, Zhao H, Wang H, Di L, et al. Gather wisdom to overcome barriers: well-designed nano-drug delivery systems for treating gliomas. *Acta Pharm Sin B* 2022;**12**:1100−25.
127. Zhu Y, Yan H. Computerized tumor boundary detection using a Hopfield neural network. *IEEE Trans Med Imag* 1997;**16**:55−67.
128. Malkanthi C, Dissanayake MB. Brain tumor boundary segmentation of MR imaging using spatial domain image processing. *Int J Innov Edu Res* 2017;**5**:1−9.
129. Chan F, Lam FK, Poon P, Zhu H, Chan K. Object boundary location by region and contour deformation. *IEE Proc* 1996;**143**:353−60.
130. Ji M, Orringer DA, Freudiger CW, Ramkissoon S, Liu X, Lau D, et al. Rapid, label-free detection of brain tumors with stimulated Raman scattering microscopy. *Sci Transl Med* 2013;**5**:201ra119.
131. Li J, Du Y, Jiang Z, Tian Y, Qiu N, Wang Y, et al. Y1 receptor ligand-based nanomicelle as a novel nanoprobe for glioma-targeted imaging and therapy. *Nanoscale* 2018;**10**:5845−51.
132. Rangayyan RM, El-Faramawy NM, Desautels JE, Alim OA. Measures of acutance and shape for classification of breast tumors. *IEEE Trans Med Imag* 1997;**16**:799−810.
133. Wu W, Wu S, Zhou Z, Zhang R, Zhang Y. 3D liver tumor segmentation in CT images using improved fuzzy C-means and graph cuts. *BioMed Res Int* 2017;**2017**:5207685.
134. Chlebus G, Schenk A, Moltz JH, van Ginneken B, Hahn HK, Meine H. Automatic liver tumor segmentation in CT with fully convolutional neural networks and object-based postprocessing. *Sci Rep* 2018;**8**:15497.
135. Zhang YM, Shi R, Hou JC, Liu ZR, Cui ZL, Li Y, et al. Liver tumor boundaries identified intraoperatively using real-time indocyanine green fluorescence imaging. *J Cancer Res Clin Oncol* 2017;**143**:51−8.
136. Chen J, Yan K, Zhang YD, Tang Y, Xu X, Sun SW, et al. Sequential learning on liver tumor boundary semantics and prognostic biomarker mining. *arXiv* 2021. Available from: https://arxiv.org/abs/2103.05170v1.
137. Yu H, Zhu GY, Xu RZ, Niu HZ, Lu Q, Li GZ, et al. Arterial embolization hyperthermia using As_2O_3 nanoparticles in VX2 carcinoma-induced liver tumors. *PLoS One* 2011;**6**:e17926.
138. Zhang C, Wang W, Liu T, Wu Y, Guo H, Wang P, et al. Doxorubicin-loaded glycyrrhetinic acid-modified alginate nanoparticles for liver tumor chemotherapy. *Biomaterials* 2012;**33**:2187−96.
139. Xue H, Qin L, Zhang L, Li X, Wu F, Wang W, et al. Preparation of docetaxel-loaded, glycyrrhetinic acid-modified nanoparticles and their liver-targeting and antitumor activity. *Exp Ther Med* 2021;**22**:1144.
140. Zong J, Peng H, Qing X, Fan Z, Xu W, Du X, et al. pH-responsive pluronic F127−lenvatinib-encapsulated halogenated boron-dipyrromethene nanoparticles for combined photodynamic therapy and chemotherapy of liver cancer. *ACS Omega* 2021;**6**:12331−42.
141. Ebadi M, Bullo S, Buskara K, Hussein MZ, Fakurazi S, Pastorin G. Release of a liver anticancer drug, sorafenib from its PVA/LDH- and PEG/LDH-coated iron oxide nanoparticles for drug delivery applications. *Sci Rep* 2020;**10**:21521.
142. Ochiai Y, Arai S, Nakao M, Shono T, Kita H. Diagnosis of boundary in early gastric cancer. *World J Gastrointest Endosc* 2012;**4**:75−9.
143. Davis RM, Kiss B, Trivedi DR, Metzner TJ, Liao JC, Gambhir SS. Surface-enhanced Raman scattering nanoparticles for multiplexed imaging of bladder cancer tissue permeability and molecular phenotype. *ACS Nano* 2018;**12**:9669−79.